

Quantum information with top quarks in QCD production

Yoav Afik^{1,*} and Juan Ramón Muñoz de Nova^{2,†}

¹*Experimental Physics Department, CERN, 1211 Geneva, Switzerland*

²*Departamento de Física de Materiales, Universidad Complutense de Madrid, E-28040 Madrid, Spain*

(Dated: March 14, 2022)

We present here the general framework to study the quantum state of a top-antitop ($t\bar{t}$) quark pair produced through quantum chromodynamics (QCD) in a high-energy collider. We show that, in general, the total quantum state that can be probed in a collider is given in terms of the production spin density matrix, which gives rise to a mixed state. We compute the quantum state of the $t\bar{t}$ pair produced from the most elementary QCD processes, finding the presence of entanglement and CHSH violation in different regions of phase space. We show that any realistic hadronic production of a $t\bar{t}$ pair is a statistical mixture of these elementary processes. We focus on the experimentally relevant cases of proton-proton and proton-antiproton collisions, performed at the LHC and the Tevatron, analyzing the dependence of the quantum state with the energy of the collisions. We provide experimentally relevant observables for entanglement and CHSH violation signatures. At the LHC, these signatures are given by the measurement of a single observable. In the case of entanglement, this signature represents the violation of a Cauchy-Schwarz inequality. We extend the quantum tomography protocol for the $t\bar{t}$ pair proposed in the literature to more general quantum states, finding that it is valid for any $t\bar{t}$ production mechanism. Finally, we argue that the CHSH violation detected in a collider is only a weak form of violation of Bell's theorem, necessarily containing a number of loopholes.

I. INTRODUCTION

The Standard Model of particle physics is a relativistic quantum field theory, based on special relativity and quantum mechanics. Therefore, it allows to test fundamental properties of quantum mechanics in a genuinely relativistic environment, at the frontier of the known Physics. However, even though the Standard Model is inherently a quantum theory, testing basic quantum phenomena in a high-energy collider can become quite challenging due to the nature of the measurement process.

Some light on this problem can be shed by the field of quantum information, where most of the foundations of quantum mechanics find a direct application. There, a characteristic signature of quantumness is provided by the existence of correlations that cannot be accounted by a classical probability theory, arising due to the intrinsic wave nature of quantum mechanics. Here emerges the concept of entanglement [1–3], perhaps the most genuine feature of quantum mechanics. Entanglement plays a key role in quantum technologies like quantum computation, cryptography, metrology and teleportation [4–10]. In particular, the study of entanglement in high-energy setups is of fundamental interest since entanglement is expected to be critically affected by relativistic effects [11–15]. A number of works have already studied the role of entanglement in the context of high-energy physics [16–21].

The simplest system which can exhibit entanglement is that formed by two qubits. In high-energy physics, an interesting realization of a two-qubit system is provided

by a pair of decaying spin-1/2 particles because their spin correlations can be measured from the kinematical distribution of their decay products. The best candidate from the Standard Model to carry out such a measurement is the top quark. The top quark is the most massive fundamental particle known to exist ($m_t c^2 \approx 173$ GeV), first discovered by the D0 and CDF collaborations at the Tevatron in Fermilab [22, 23]. Top quarks are typically produced in top-antitop ($t\bar{t}$) pairs which, due to their high mass, quickly decay well before any other process can affect their spin correlations. The spins of the $t\bar{t}$ pair determine the kinematics of the decay products, from where the original top spin quantum state can be reconstructed.

This feature has rendered top spin correlations a rich subject of study within high-energy physics [24–31]. Indeed, spin correlations between $t\bar{t}$ pairs have already been measured by the D0 and CDF collaborations at the Tevatron with proton-antiproton ($p\bar{p}$) collisions [32–34], and by the ATLAS and CMS collaborations at the Large Hadron Collider (LHC) with proton-proton (pp) collisions [35–39].

However, despite the extensive literature on the topic, only a very recent work has studied the entanglement between $t\bar{t}$ pairs [40]. In particular, it was proposed that the entanglement of a $t\bar{t}$ pair can be detected at the LHC with high statistical significance using the current data recorded during Run 2. This would represent the first measurement ever of entanglement in a quark pair, and the highest-energy observation of entanglement so far. An experimental protocol for the quantum tomography of a $t\bar{t}$ pair was also developed in Ref. [40], a canonical technique in quantum information but novel in the high-energy context. In parallel, some recent works have also addressed the possibility of measuring the vi-

* yoavafik@gmail.com

† jrmnova@fis.ucm.es

olation of Bell inequalities with $t\bar{t}$ pairs [41, 42], and also with W^+W^- pairs [43], which are massive spin-1 bosons. Even the measurement of such a basic quantum phenomenon as quantum interference can become non-trivial in a high-energy collider [44]. Apart from the intrinsic interest of testing foundational aspects of quantum mechanics at the frontier of the known Physics, all these works are paving the way to use high-energy colliders also for the study of quantum information theory. Due to their genuine relativistic behavior, the exotic character of the symmetries and interactions involved, as well as their fundamental nature, high-energy colliders are extremely attractive systems for these purposes.

Here, we extend the analysis of Ref. [40] to provide the general formalism to study the quantum state of $t\bar{t}$ pairs created through quantum chromodynamics (QCD) within a genuine quantum information approach. We discuss that, in general, the total quantum state that can be probed in a scattering experiment in a collider is given in terms of the so-called production spin density matrix (PM) [25], which is necessarily a mixed state.

For the specific case of a $t\bar{t}$ pair, we study in detail its quantum state for the most elementary QCD production processes: light quark-antiquark ($q\bar{q}$) or gluon-gluon (gg) interactions. We generalize the entanglement analysis of Ref. [40] including also the violation of Bell inequalities, finding their emergence in certain regions of phase space for both $q\bar{q}$ and gg processes. Interestingly, the entanglement structure can be qualitatively understood in terms of basic conservation laws, without the need of knowledge of the particular details of QCD interactions. We show that any realistic QCD mechanism of $t\bar{t}$ production can be studied in terms of a statistical mixture of the previous building blocks. In particular, we focus on the case of pp and $p\bar{p}$ collisions, corresponding to the LHC and the Tevatron, respectively. We study the dependence of the quantum state on the energy of the collisions, finding that for sufficiently high energies both types of collision converge to the same state due to the dominance of gg processes.

We review how spin correlations are measured in a high-energy collider, obtained from the fit of the differential cross-section describing the angular distribution of the decay products. From there, we propose realistic experimental observables for the characterization of the $t\bar{t}$ quantum state by integrating the signal in certain regions of phase space. At the LHC, it was shown [40] that an entanglement signature can be obtained from the measurement of one single magnitude, proportional to the trace of the spin correlation matrix. We show here that a signature of violation of Bell inequality is also provided by just measuring one parameter, the transverse spin correlations. Moreover, we carry out a study of the energy dependence of both signatures. Regarding the Tevatron, we find that an entanglement signature is provided by directly integrating the signal in whole phase space.

Finally, we analyze in detail the conceptual significance of the experimental implementation of these techniques.

We show explicitly that an entanglement measurement at the LHC represents the violation of a Cauchy-Schwarz inequality. In contrast, we do not expect a statistically significant observation of entanglement at the Tevatron. We discuss that the quantum tomography protocol developed in Ref. [40] can be extended to any $t\bar{t}$ production process. We argue that, due to the nature of the detection process, only weak violations of Bell inequalities can be measured in a high-energy collider, since some loopholes, like those related to the free-will or to the detection efficiency, cannot be closed.

Remarkably, while the probability and the PM of each production process is computed by the high-energy theory, once given we are simply left with a typical problem in quantum information involving two-qubit quantum states, where the usual techniques of the field can be applied. This important observation is translated into the article presentation, fully developed within a quantum information language, aimed at making it easily understandable by the physics community outside the high-energy field.

The paper is arranged as follows. Section II discusses in detail the general framework upon we build the results of this work, presenting the basic tools of two-qubit systems used throughout this work along with a general discussion about quantum states in colliders and relativistic particle/antiparticle production. Section III studies the $t\bar{t}$ quantum state in fundamental QCD processes. Section IV extends the previous results to more realistic processes occurring in actual colliders, analyzing in detail the energy dependence. Section V translates these ideas into relevant experimental observables. Section VI provides some technical remarks about the experimental implementation of the discussed quantum information techniques. Finally, Section VII summarizes the main conclusions and discusses future perspectives. Technical details are provided in the Appendices.

II. GENERAL FORMALISM

A. Spin-1/2 systems

Quantum states are represented in general by a density matrix ρ , a Hermitian non-negative operator with unit trace in a certain Hilbert space \mathcal{H} , $\text{tr}(\rho) = 1$. These conditions imply that the number of real parameters characterizing ρ for $\dim \mathcal{H} = N$ is $N^2 - 1$. Expectation values for observables O are computed by taking the product trace, $\langle O \rangle = \text{tr}(O\rho)$.

The most simple example of density matrix is provided by a qubit, i.e., a two-level quantum system. The density matrix takes the simple form

$$\rho = \frac{I_2 + \sum_i B_i \sigma^i}{2} \quad (1)$$

where I_n is the $n \times n$ identity matrix and σ^i , $i = 1, 2, 3$, the usual Pauli matrices. A physical (i.e., non-negative)

density matrix ρ is described by vectors $|\mathbf{B}| \leq 1$, with pure states given by unit vectors saturating the inequality. The 3 coefficients B_i completely determine the quantum state of the system. For a spin-1/2 particle, they represent the spin polarization, $B_i = \langle \sigma^i \rangle$. An alternative description of ρ can be provided in terms of angular momentum coherent states $|\hat{\mathbf{n}}\rangle$ through the P -representation (see Appendix A for a summary of its main properties)

$$\rho = \int d\Omega P(\hat{\mathbf{n}}) |\hat{\mathbf{n}}\rangle \langle \hat{\mathbf{n}}|, \int d\Omega P(\hat{\mathbf{n}}) = 1 \quad (2)$$

where the angular momentum coherent states $|\hat{\mathbf{n}}\rangle$ satisfy $\hat{\mathbf{n}} \cdot \sigma |\hat{\mathbf{n}}\rangle = |\hat{\mathbf{n}}\rangle$, and Ω is the solid angle associated to the unit vector $\hat{\mathbf{n}}$. The function $P(\hat{\mathbf{n}})$ is the spin-1/2 analogue of the celebrated Glauber-Sudarshan P -function in quantum optics [45]. It is easily seen that $P(\mathbf{n})$ can be always chosen as non-negative for any density matrix ρ describing a qubit.

More intriguing quantum states arise in bipartite Hilbert spaces $\mathcal{H} = \mathcal{H}_A \otimes \mathcal{H}_B$ composed of subsystems A, B . A quantum state is called separable iff it can be written as a convex sum of product states

$$\rho = \sum_n p_n \rho_n^A \otimes \rho_n^B, \quad (3)$$

with $p_n \geq 0$. An entangled state is defined as a non-separable state.

To illustrate this concept, we consider the case of a pair of qubits, where any density matrix ρ can be decomposed as

$$\rho = \frac{I_4 + \sum_i (B_i^+ \sigma^i \otimes I_2 + B_i^- I_2 \otimes \sigma^i) + \sum_{i,j} C_{ij} \sigma^i \otimes \sigma^j}{4} \quad (4)$$

Now, the quantum state of the system is determined by 15 parameters B_i^\pm, C_{ij} , which for spin-1/2 particles are their spin polarizations $B_i^+ = \langle \sigma^i \otimes I_2 \rangle, B_i^- = \langle I_2 \otimes \sigma^i \rangle$, and their spin correlations $C_{ij} = \langle \sigma^i \otimes \sigma^j \rangle$.

An insightful way to understand entanglement for 2-qubit systems arises by considering the P -representation

$$\rho = \int d\Omega_A d\Omega_B P(\mathbf{n}_A, \mathbf{n}_B) |\mathbf{n}_A \mathbf{n}_B\rangle \langle \mathbf{n}_A \mathbf{n}_B|, \quad (5)$$

where $|\mathbf{n}_A \mathbf{n}_B\rangle = |\mathbf{n}_A\rangle \otimes |\mathbf{n}_B\rangle$. From Eq. (3), it is immediately seen that a state is separable iff it admits a non-negative P -representation. This implies that the spin correlations for a separable state

$$C_{ij} = \langle \sigma^i \otimes \sigma^j \rangle = \int d\Omega_A d\Omega_B P(\mathbf{n}_A, \mathbf{n}_B) n_A^i n_B^j \quad (6)$$

are purely classical, described by a classical probability distribution. The same applies to the spin polarizations. Thus, in the language of the P -function, entanglement is equivalent to a $P(\mathbf{n}_A, \mathbf{n}_B)$ function that necessarily presents negative values, a genuine distinctive signature of non-classicality and quantum behavior, as well known in quantum optics [45].

In order to signal the presence of entanglement, several theoretical criteria can be used. Perhaps the most well-known one is the Peres-Horodecki criterion [46, 47], which simply states that if ρ is separable, taking partial transpose with respect to the second subsystem

$$\rho^{\text{T}_2} = \sum_n p_n \rho_n^a \otimes (\rho_n^b)^{\text{T}}, \quad (7)$$

also yields a non-negative operator. Hence, a not non-negative ρ^{T_2} implies that ρ is entangled. In two-qubit systems, the Peres-Horodecki criterion is also a necessary condition for entanglement.

A quantitative measurement of the entanglement of two qubits is provided by the concurrence [48]

$$C[\rho] \equiv \max(0, \lambda_1 - \lambda_2 - \lambda_3 - \lambda_4) \quad (8)$$

with λ_i the eigenvalues of the matrix $\sqrt{\sqrt{\rho} \tilde{\rho} \sqrt{\rho}}$ ordered in decreasing magnitude, $\tilde{\rho} = (\sigma_2 \otimes \sigma_2) \rho^* (\sigma_2 \otimes \sigma_2)$, and ρ^* the complex conjugate of ρ in the spin basis of σ_3 . The concurrence satisfies $0 \leq C[\rho] \leq 1$ and is related to the entanglement of formation, where a quantum state is entangled iff $C[\rho] > 0$. Hence, $C[\rho] = 1$ implies that ρ is maximally entangled.

The implementation of these techniques requires full knowledge of the quantum state. This can be achieved by means of the quantum tomography, which is able to reconstruct a quantum state from the measurement of a selected set of observables. For the case of a single qubit, characterized by 3 parameters, it is enough to measure the vector \mathbf{B} , which is the spin polarization for a spin-1/2 particle. For the case of two qubits, the quantum tomography is performed by measuring the 15 parameters of $\mathbf{B}^\pm, \mathbf{C}$, which for spin-1/2 particles represent the spin polarizations and spin correlations, respectively. In actual experiments, an additional measurement is typically required to ensure the proper normalization of the density matrix [49].

Nevertheless, in order to detect entanglement, simpler criteria can be adapted, which require the measurement of just a few parameters. Appendix B contains some entanglement criteria that are specifically developed for $t\bar{t}$ quantum states and used throughout this work.

An even stronger requirement than entanglement is the violation of Bell-type inequalities [3]. No local hidden-variable model can give rise to it, implying a violation of local realism. The Clauser-Horne-Shimony-Holt (CHSH) inequality [50] provides a particularly useful realization of Bell inequality for 2×2 systems:

$$|C(a_1, b_1) - C(a_1, b_2) + C(a_2, b_1) + C(a_2, b_2)| \leq 2 \quad (9)$$

where $a_i, b_i, i = 1, 2$ represent measurement settings in the Alice, Bob subsystems A, B , respectively, and $C(a_i, b_j)$ are their correlations. In the case of spin-1/2 particles, they can be interpreted as measurement settings of spin polarizations along certain directions given by unit vectors $\mathbf{a}_i, \mathbf{b}_j$, $C(a_i, b_j) = \langle (\mathbf{a}_i \cdot \sigma) \otimes (\mathbf{b}_j \cdot \sigma) \rangle$.

Thus, Eq. (9) can be rewritten in vector notation as simply

$$|\mathbf{a}_1^T \mathbf{C} (\mathbf{b}_1 - \mathbf{b}_2) + \mathbf{a}_2^T \mathbf{C} (\mathbf{b}_1 + \mathbf{b}_2)| \leq 2 \quad (10)$$

with \mathbf{C} the correlation matrix of Eq. (4). Any separable state of the form (3) satisfies Eq. (10). Hence, only entangled states can violate a CHSH inequality.

In practice, the maximization of the l.h.s. of Eq. (10) is computed from

$$\mathcal{B}[\rho] \equiv \max_{\mathbf{a}_i, \mathbf{b}_i} |\mathbf{a}_1^T \mathbf{C} (\mathbf{b}_1 - \mathbf{b}_2) + \mathbf{a}_2^T \mathbf{C} (\mathbf{b}_1 + \mathbf{b}_2)| = 2\sqrt{\mu_1 + \mu_2} \quad (11)$$

where $0 \leq \mu_i \leq 1$ are the eigenvalues of $\mathbf{C}^T \mathbf{C}$, ordered in decreasing magnitude [51]. Therefore, the CHSH inequality can be violated iff $\mu_1 + \mu_2 > 1$, where the maximum possible violation of the CHSH inequality is the Cirel'son bound $\mathcal{B}[\rho] = 2\sqrt{2}$ [52].

B. Quantum states in colliders

We now study how the physics in real colliders can be described in terms of quantum states. For illustrative purposes, we first address the simple non-relativistic scattering of an incident spinless particle with mass m from a single fixed target, described by a potential V (the interested reader is referred to Ref. [53] for the basics of scattering theory). The process is determined by the scattering matrix S , whose elements in momentum representation are

$$\langle \mathbf{p}' | S | \mathbf{p} \rangle = \delta(\mathbf{p} - \mathbf{p}') - 2\pi i \delta(E_{\mathbf{p}'} - E_{\mathbf{p}}) \langle \mathbf{p}' | T | \mathbf{p} \rangle \quad (12)$$

where the T -matrix satisfies the Lippmann-Schwinger equation $T = V + VG_0T$, with G_0 the usual retarded free Green's function, and $E_{\mathbf{p}} = \mathbf{p}^2/2m$ the kinetic energy. The scattering amplitude $f(\mathbf{p} \rightarrow \mathbf{p}') \equiv -(2\pi)^2 m \hbar \langle \mathbf{p}' | T | \mathbf{p} \rangle$ determines the differential cross-section characterizing the scattering of an initial state with momentum \mathbf{p} to some momentum $\hat{\mathbf{p}'}$

$$\frac{d\sigma}{d\Omega} = |f(\mathbf{p} \rightarrow \mathbf{p}')|^2 \quad (13)$$

Ω being the solid angle associated to \mathbf{p}' . Therefore, the differential cross-section is proportional to the probability of the process, given by the squared *on-shell* T -matrix element connecting the initial to the final state.

The wave function describing the scattered state from an incident particle with well-defined momentum $|\mathbf{p}\rangle$ is

$$|\Psi\rangle = S |\mathbf{p}\rangle \quad (14)$$

which can be rewritten as a density matrix

$$\rho_S = |\Psi\rangle \langle \Psi| = \iint d\mathbf{p}' d\mathbf{p}'' |\mathbf{p}'\rangle \langle \mathbf{p}'| S |\mathbf{p}\rangle \langle \mathbf{p}| S^\dagger |\mathbf{p}''\rangle \langle \mathbf{p}''| \quad (15)$$

However, in a real collider, only momentum measurements of the scattered particle can be performed and thus, not all the information is needed to describe the relevant quantum state for experiments. Moreover, scattering events along the beam direction are not typically measured. Therefore, the relevant quantum state that encodes all the information that can be probed in a collider results from projecting ρ_S onto momentum states $\mathbf{p}' \neq \mathbf{p}$ with the operators $\Pi_{\mathbf{p}'} = |\mathbf{p}'\rangle \langle \mathbf{p}'|$ as

$$\begin{aligned} \rho &= \frac{\int d\mathbf{p}' \Pi_{\mathbf{p}'} |\Psi\rangle \langle \Psi| \Pi_{\mathbf{p}'}}{\int d\mathbf{p}' |\langle \Psi | \mathbf{p}' \rangle|^2 \langle \mathbf{p}' | \mathbf{p}' \rangle} = \frac{\int d\Omega |\langle \mathbf{p}' | T | \mathbf{p} \rangle|^2 |\mathbf{p}'\rangle \langle \mathbf{p}'|}{\int d\Omega |\langle \mathbf{p}' | T | \mathbf{p} \rangle|^2 \langle \mathbf{p}' | \mathbf{p}' \rangle} \\ &= \frac{1}{\sigma} \int d\Omega \frac{d\sigma}{d\Omega} \frac{|\mathbf{p}'\rangle \langle \mathbf{p}'|}{\langle \mathbf{p}' | \mathbf{p}' \rangle} = \frac{1}{\sigma} \int d\sigma \frac{|\mathbf{p}'\rangle \langle \mathbf{p}'|}{\langle \mathbf{p}' | \mathbf{p}' \rangle} \end{aligned} \quad (16)$$

where the factor $\langle \mathbf{p}' | \mathbf{p}' \rangle = \delta(\mathbf{0})$ in the denominator ensures proper normalization, $\text{tr } \rho = 1$. The quantum state ρ is thus a mixed resulting from the incoherent sum of momentum states with a probability proportional to the differential cross-section, where the total cross-section here plays an analogue role to the partition function in statistical mechanics. As a result, we have a density matrix written only in terms of differential cross-sections, which are the observables measured in actual colliders, computed in terms of T -matrix elements. In this way, the expectation value of any momentum observable $O(\mathbf{P})$ reads

$$\langle O \rangle = \text{tr}[O\rho] = \frac{1}{\sigma} \int d\sigma O(\mathbf{p}') \quad (17)$$

For a spin-half particle, things go along the same lines. By noticing that the spin of the scattered particle is not typically detected in a collider, we now project as $\Pi_{\mathbf{p}'} = \sum_{\alpha} |\mathbf{p}'\alpha\rangle \langle \mathbf{p}'\alpha|$, where α labels spin indices, finding that the quantum state characterizing the scattering of an incident particle with momentum \mathbf{p} and spin λ is

$$\begin{aligned} \rho^{\lambda} &= \frac{1}{Z} \sum_{\alpha\beta} \int d\Omega \langle \mathbf{p}'\alpha | T | \mathbf{p}\lambda \rangle \langle \mathbf{p}\lambda | T^\dagger | \mathbf{p}'\beta \rangle \frac{|\mathbf{p}'\alpha\rangle \langle \mathbf{p}'\beta|}{\langle \mathbf{p}' | \mathbf{p}' \rangle} \\ &= \frac{1}{Z} \sum_{\alpha\beta} \int d\Omega R_{\alpha\beta}^{\lambda}(\mathbf{p}') \frac{|\mathbf{p}'\alpha\rangle \langle \mathbf{p}'\beta|}{\langle \mathbf{p}' | \mathbf{p}' \rangle} \end{aligned} \quad (18)$$

where the partition function Z is defined to ensure normalization and the production spin density matrix is defined as

$$R_{\alpha\beta}^{\lambda}(\mathbf{p}') \equiv \langle \mathbf{p}'\alpha | T | \mathbf{p}\lambda \rangle \langle \mathbf{p}\lambda | T^\dagger | \mathbf{p}'\beta \rangle \quad (19)$$

The PM is not properly normalized, since its trace is proportional to the differential cross-section of the process

$$\text{tr } R^{\lambda}(\mathbf{p}') = \sum_{\alpha} R_{\alpha\alpha}^{\lambda}(\mathbf{p}') = \sum_{\alpha} |\langle \mathbf{p}'\alpha | T | \mathbf{p}\lambda \rangle|^2 \propto \frac{d\sigma^{\lambda}}{d\Omega} \quad (20)$$

The proportionality factor can be chosen arbitrarily; for the present moment, we take R^{λ} directly proportional

to the on-shell T -matrix elements. Thus, the partition function is once more proportional to the cross-section

$$Z = \int d\Omega \operatorname{tr} R^\lambda(\mathbf{p}') \propto \int d\Omega \frac{d\sigma^\lambda}{d\Omega} = \int d\sigma^\lambda = \sigma^\lambda \quad (21)$$

As a 2×2 Hermitian matrix, the most general form of the PM is

$$R^\lambda = \tilde{A}^\lambda + \sum_i \tilde{B}_i^\lambda \sigma^i \quad (22)$$

Thus, the PM has a similar form to that of Eq. (1), but with an extra parameter \tilde{A}^λ that determines the differential cross-section of the process, associated to the probability of the process, $\operatorname{tr} R^\lambda(\mathbf{p}') = 2\tilde{A}^\lambda(\mathbf{p}')$.

The proper density matrix with unit trace describing the quantum state for a scattering process along a certain direction is obtained by normalization of R ,

$$\rho_{\alpha\beta}^\lambda(\mathbf{p}') = \frac{R_{\alpha\beta}^\lambda(\mathbf{p}')}{\operatorname{tr} R^\lambda(\mathbf{p}')} = \frac{R_{\alpha\beta}^\lambda(\mathbf{p}')}{2\tilde{A}^\lambda(\mathbf{p}')} \quad (23)$$

whose spin polarization is given by $B_i = \tilde{B}_i^\lambda/\tilde{A}^\lambda$. In terms of these quantum substates, the total quantum state of Eq. (24) can be written as simply

$$\rho^\lambda = \frac{1}{\sigma^\lambda} \sum_{\alpha\beta} \int d\sigma^\lambda \rho_{\alpha\beta}^\lambda(\mathbf{p}') \frac{|\mathbf{p}'\alpha\rangle\langle\mathbf{p}'\beta|}{\langle\mathbf{p}'|\mathbf{p}'\rangle} \quad (24)$$

Hence, we can intuitively understand the total quantum state ρ^λ as the incoherent combination of the quantum states describing the scattering of the incident particle along a certain direction, weighted with the probability of that scattering process, proportional to the differential cross section, with the total cross-section σ^λ playing the role once more of the partition function.

Finally, we note that in a collider the initial state is typically unpolarized since spin degrees of freedom cannot be controlled. Thus, the real quantum state describing the experimental after many events results from the averaged PM

$$R(\mathbf{p}') = \frac{1}{2} \sum_\lambda R^\lambda(\mathbf{p}') \quad (25)$$

In summary, the quantum state describing the scattered particles in a collider is a mixed state because of two fundamentally different reasons, related to the measurement process and the control over degrees of freedom. (i) Regarding orbital variables: Momentum distributions of the scattered particles are the only measurable observables in high-energy colliders, given in terms of differential cross-sections. Thus, even if the scattered state is pure, one can only access to the diagonal part in momentum, which motivates the use of a reduced mixed density matrix. (ii) Regarding discrete variables: Internal degrees of freedom of the initial state cannot be typically controlled and one has to average uniformly (in principle) over them. The average over all possible initial states after many scattering events results in an incoherent mixture that is described by a density matrix.

C. Relativistic particle/antiparticle pair production

We now switch to the actual case of high-energy colliders, whose physics is described by relativistic quantum field theories within the framework of the Standard Model. The Standard Model is composed of fundamental spin-1/2 particles (and their corresponding antiparticles) which interact through the mediation of gauge bosons of spin-1. These interactions can be either strong (mediated by massless gluons g), weak (mediated by the massive Z^0, W^\pm bosons), or electromagnetic (mediated by the photon γ), corresponding to a Yang-Mills theory $SU(3) \otimes SU(2) \otimes U(1)$, respectively. Electromagnetic and weak interactions are both unified within the framework of electroweak theory, while strong interactions are described by quantum chromodynamics. The remaining particle of the Standard Model, the Higgs boson, has spin-0 and is the responsible for the occurrence of mass in massive particles.

A natural Standard Model candidate for an entangled two-qubit system is a particle-antiparticle (denoted generically as $P\bar{P}$) pair produced from some initial state I

$$I \rightarrow P + \bar{P} \quad (26)$$

In the following, we restrict to the case where P is a Standard Model fermion of mass m , although the formalism can be easily generalized to the case where P is some massless spin-1 gauge boson like the photon. Among the Standard Model fermions, we can distinguish between quarks and leptons, where the latter do not interact through QCD since they do not have color degrees of freedom. Typically, the components of the initial state I annihilate themselves through these gauge interactions, giving rise to the $P\bar{P}$ pair. In the process, the total energy and momentum of the initial state is conserved.

The kinematics of a $P\bar{P}$ pair is determined in the center-of-mass (c.m.) frame by the invariant mass M and the direction of flight \hat{k} of the particle P . In this frame, the particle/antiparticle four-momenta read $k^\mu = (k^0, \mathbf{k}), \bar{k}^\mu = (k^0, -\mathbf{k})$, with $\hat{k} = \mathbf{k}/|\mathbf{k}|$, which satisfy the Lorentz-invariant dispersion relation

$$\bar{k}^2 = k^2 \equiv k^\mu k_\mu = (k^0)^2 - \mathbf{k}^2 = m^2, \quad (27)$$

where in the following we work in natural units $\hbar = c = 1$.

The invariant mass M is the c.m. energy of the pair, defined from the usual invariant Mandelstam variables as

$$M^2 \equiv s \equiv (k + \bar{k})^2, \quad (28)$$

In the c.m. frame, $M^2 = 4(k^0)^2 = 4(m^2 + \mathbf{k}^2)$, which is related to the top c.m. frame velocity β by $|\mathbf{k}| = m\beta/\sqrt{1 - \beta^2}$, so

$$\beta = \sqrt{1 - 4m^2/M^2}, \quad (29)$$

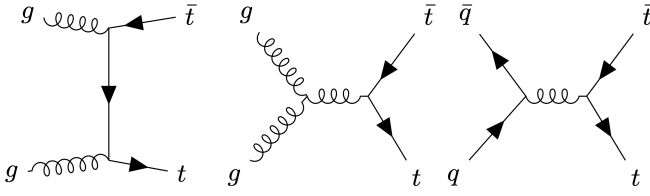


FIG. 1. Representative Feynman diagrams for $t\bar{t}$ production within the Standard Model. Spring lines represent gluons and straight lines represent quarks, all either real or virtual.

Hence, threshold production ($\beta = 0$) is at the minimum energy possible for a $P\bar{P}$ pair, $M = 2m$, as naturally expected.

With respect to the quantum state of the $P\bar{P}$ pair, *mutatis mutandis*, we define again a PM in terms of the *on-shell* relativistic T -matrix elements as

$$R_{\alpha\beta,\alpha'\beta'}^{I\lambda}(M, \hat{k}) \equiv \langle M\hat{k}\alpha\beta | T | I\lambda \rangle \langle I\lambda | T^\dagger | M\hat{k}\alpha'\beta' \rangle \quad (30)$$

with $|I\lambda\rangle$ labeling the initial state of the system and

$$|M\hat{k}\alpha\beta\rangle \equiv |k\alpha\rangle \otimes |\bar{k}\beta\rangle \quad (31)$$

where the first/second subspace correspond to the particle/antiparticle, respectively. The spins of the particles are computed in their respective rest frames, where they are well defined. Once more, if internal degrees of freedom λ of the initial state cannot be controlled (like spin or color), one uses the averaged PM

$$R_{\alpha\beta,\alpha'\beta'}^I(M, \hat{k}) = \frac{1}{N_\lambda} \sum_\lambda R_{\alpha\beta,\alpha'\beta'}^{I\lambda}(M, \hat{k}) \quad (32)$$

with $N_{I\lambda}$ the number of internal degrees of freedom of I . In analogy to Eq. (24), the resulting quantum state is

$$Z = \frac{1}{Z} \sum_{\alpha\beta,\alpha'\beta'} \int d\Omega R_{\alpha\beta,\alpha'\beta'}^I(M, \hat{k}) \frac{|M\hat{k}\alpha\beta\rangle \langle M\hat{k}\alpha'\beta'|}{\langle M\hat{k}|M\hat{k} \rangle} \quad (33)$$

with the the partition function Z proportional once more to the total cross-section

$$Z = \int d\Omega \text{tr } R^I(M, \hat{k}) \propto \sigma^I \quad (34)$$

The PM characterizes the quantum state of any $P\bar{P}$ pair produced in a relativistic process, which is a mixed state by the very same reasons as in the non-relativistic case. It takes the general form

$$R = \tilde{A}I_4 + \sum_i \left(\tilde{B}_i^+ \sigma^i \otimes I_2 + \tilde{B}_i^- I_2 \otimes \sigma^i \right) + \sum_{i,j} \tilde{C}_{ij} \sigma^i \otimes \sigma^j \quad (35)$$

in a similar fashion to Eq. (4), but once more with an extra coefficient \tilde{A} proportional to the c.m. differential cross-section.

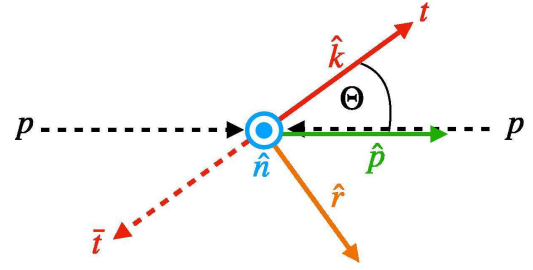


FIG. 2. Orthonormal helicity basis, defined in the c.m. frame. \hat{k} is the direction of the top and \hat{p} the direction of the initial beam. The vector \hat{n} is perpendicular to the $\{\hat{k}, \hat{p}\}$ plane and $\hat{r} = \hat{k} \times \hat{n}$ is the vector orthogonal to \hat{k} in the $\{\hat{k}, \hat{p}\}$ plane.

The actual spin density matrix describing the spin quantum state of the system is obtained from the normalization of R ,

$$\rho = \frac{R}{\text{tr}(R)} = \frac{R}{4\tilde{A}} \quad (36)$$

As a result, the spin polarizations B_i^\pm and spin correlations C_{ij} of the $P\bar{P}$ pair are

$$B_i^\pm = \frac{\tilde{B}_i^\pm}{\tilde{A}}, \quad C_{ij} = \frac{\tilde{C}_{ij}}{\tilde{A}} \quad (37)$$

In terms of these quantum states, we retrieve the relativistic version of Eq. (24),

$$\rho^I = \frac{1}{\sigma^I} \sum_{\alpha\beta,\alpha'\beta'} \int d\Omega \rho_{\alpha\beta,\alpha'\beta'}^I(M, \hat{p}) \frac{|M\hat{k}\alpha\beta\rangle \langle M\hat{k}\alpha'\beta'|}{\langle M\hat{k}|M\hat{k} \rangle} \quad (38)$$

III. PRODUCTION OF $t\bar{t}$ IN FUNDAMENTAL QCD PROCESSES

A particularly interesting example of particle-antiparticle pair is provided by a top-antitop quark pair, which will be the subject of study throughout the rest of the work. Specifically, we restrict to the production of $t\bar{t}$ pairs through QCD processes, although the concepts and techniques developed here can be straightforwardly extended to other types of interaction and/or other particle-antiparticle pairs. For the theoretical computations, we employ leading-order (LO) QCD perturbation theory since it provides analytical results and a clear picture of the underlying physics. Higher-order corrections are known to be small and do not change the main results [28, 40–42].

At LO QCD, only two initial states can produce a $t\bar{t}$ pair: a light quark-antiquark ($q\bar{q}$) or a gluon (gg) pair,

$$\begin{aligned} q + \bar{q} &\rightarrow t + \bar{t}, \\ g + g &\rightarrow t + \bar{t}. \end{aligned} \quad (39)$$

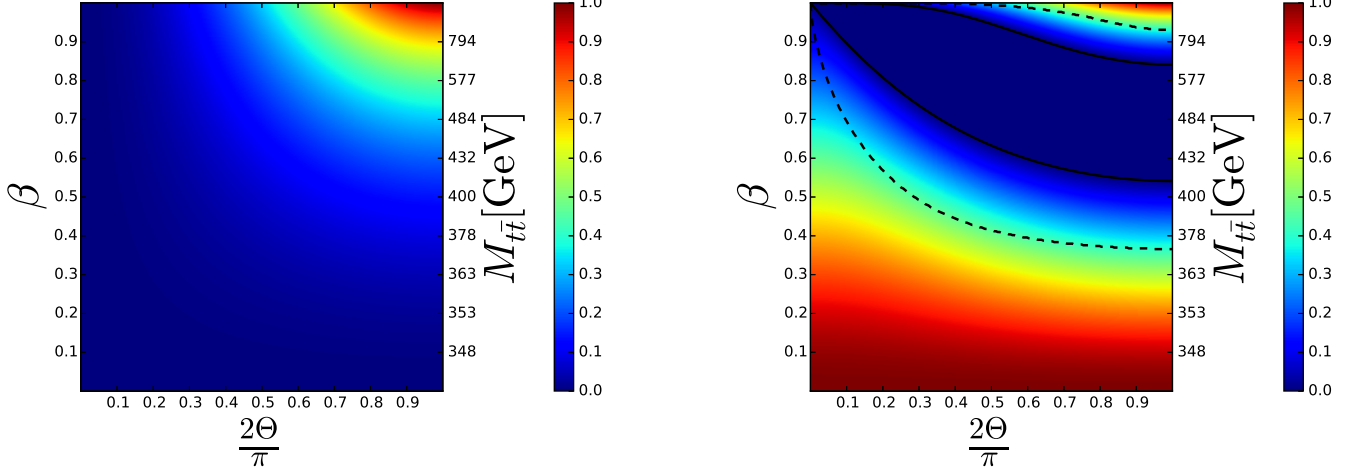


FIG. 3. Concurrence of the spin density matrix $\rho^I(\beta, \hat{k})$ resulting from an initial state $I = q\bar{q}, gg$ as a function of the top velocity β and the production angle Θ in the $t\bar{t}$ c.m. frame. All plots are symmetric under the transformation $\Theta \rightarrow \pi - \Theta$. Left: $q\bar{q} \rightarrow t\bar{t}$. Right: $gg \rightarrow t\bar{t}$. Solid black lines represent the critical boundaries between separability and entanglement $\beta_{c1,c2}^{\text{PH}}(\Theta)$, while dashed black lines represent the critical boundaries for the violation of the CHSH inequality, $\beta_{c1,c2}^{\text{CH}}(\Theta)$.

Representative Feynman diagrams for these processes in the Standard Model are depicted in Fig. 1.

Each initial state $I = q\bar{q}, gg$ creates a $t\bar{t}$ pair in a spin quantum state described by an averaged PM $R^I(M_{t\bar{t}}, \hat{k})$, where the spin and color degrees of freedom of the initial state have already been averaged, $M_{t\bar{t}}$ is the invariant mass of the $t\bar{t}$ pair and \hat{k} the flight direction of the top quark. For the characterization of the PM, an orthonormal basis needs to be fixed in order to compute the corresponding spin polarizations and correlations. The most common choice is the helicity basis [30], defined in the c.m. frame as $\{\hat{k}, \hat{n}, \hat{r}\}$, with $\hat{r} = (\hat{p} - \cos \Theta \hat{k}) / \sin \Theta$, $\hat{n} = \hat{r} \times \hat{k}$, where \hat{p} is a unitary vector along the direction of the initial state and Θ is the production angle of the top quark with respect to the beam, $\cos \Theta = \hat{k} \cdot \hat{p}$. We note here that, due to momentum conservation, the c.m. frame of the initial state is the same as that of the $t\bar{t}$ pair.

The advantage of the helicity basis is that, although the $t\bar{t}$ relativistic spins are only well-defined in their respective rest frames, those are equivalent to the c.m. frame via a Lorentz transformation along the top direction, which does not change the orientation of the helicity basis. A schematic representation of this basis is provided in Fig. 2.

The PM $R^I(M_{t\bar{t}}, \hat{k})$ in the helicity basis is only a function of β (or, equivalently, of $M_{t\bar{t}}$) and $\cos \Theta$. Specifically, in the SM, the correlation matrix \tilde{C}_{ij}^I is symmetric and $\tilde{B}_i^{I,+} = \tilde{B}_i^{I,-}$. Furthermore, at LO, the $t\bar{t}$ pair is unpolarized, $\tilde{B}_i^{I,\pm} = 0$, and, in QCD production, their spins along the n -axis are uncorrelated with respect to the remaining directions, $\tilde{C}_{nr}^I = \tilde{C}_{nk}^I = 0$ [38]. Therefore, $R^I(M_{t\bar{t}}, \hat{k})$ is characterized at LO QCD by only 5

parameters in the helicity basis: $\tilde{A}^I, \tilde{C}_{kk}^I, \tilde{C}_{nn}^I, \tilde{C}_{rr}^I, \tilde{C}_{kr}^I$. The values of those coefficients can be computed analytically and are easily found in the usual literature on the subject [27, 29, 30]. Here, we fix the normalization of $R^I(M_{t\bar{t}}, \hat{k})$ such that the c.m. differential cross-section for $t\bar{t}$ production from an initial state I is [27]

$$\frac{d\sigma^I}{d\Omega} = \frac{\alpha_s^2 \beta}{M_{t\bar{t}}^2} \tilde{A}^I(M_{t\bar{t}}, \hat{k}) \quad (40)$$

with $\alpha_s \approx 0.118$ the strong coupling constant characterizing the strength of QCD interactions.

The actual spin density matrices $\rho^I(M_{t\bar{t}}, \hat{k})$ are computed from the normalization of $R^I(M_{t\bar{t}}, \hat{k})$. As a result of the above considerations, at LO $\rho^I(M_{t\bar{t}}, \hat{k})$ is unpolarized, its correlation matrix is symmetric, and it is already diagonal in the \hat{n} direction. These last two properties imply that the correlation matrix can be diagonalized by an appropriated rotation in the $\{\hat{k}, \hat{r}\}$ plane, with eigenvalues C_{nn}^I and

$$C_{\pm}^I = \frac{C_{kk}^I + C_{rr}^I}{2} \pm \sqrt{\left(\frac{C_{kk}^I - C_{rr}^I}{2}\right)^2 + C_{kr}^{I2}} \quad (41)$$

We will refer to this orthonormal basis as the *diagonal* basis, characterized by unit vectors $\{\hat{u}_+, \hat{n}, \hat{u}_-\}$ with eigenvalues $\{C_+^I, C_{nn}^I, C_-^I\}$.

Regarding entanglement, since $C_{nn}^I < 0$ in all phase space and for both initial states [see Eqs. (45), (51)], we find that the Peres-Horodecki criterion is equivalent to $\Delta^I > 0$ (see Appendix B), where [54]

$$\Delta^I \equiv \frac{-C_{nn}^I + |C_+^I + C_-^I| - 1}{2} = \frac{-C_{nn}^I + |C_{kk}^I + C_{rr}^I| - 1}{2} \quad (42)$$

The concurrence is simply related to Δ^I as

$$C[\rho^I] = \max(\Delta^I, 0) \quad (43)$$

Previous approaches in high-energy physics based on the entanglement entropy [20, 55, 56] are not useful here since they are only valid for pure states. We stress that the entanglement of the quantum state $\rho^I(M_{t\bar{t}}, \hat{k})$ is Lorentz invariant since it has well-defined momentum [11, 12].

Regarding the violation of the CHSH inequality, from Eq. (11) it is immediately seen in the diagonal basis to be equivalent to

$$\mu^I \equiv C_+^{I2} + C_-^{I2} + C_{nn}^{I2} - C_{\min}^{I2} - 1 > 0 \quad (44)$$

with $C_{\min}^{I2} \equiv \min\{C_+^{I2}, C_{nn}^{I2}, C_-^{I2}\}$.

A. $q\bar{q}$ production

For $q\bar{q}$ production, the coefficients of the PM in the helicity basis are

$$\begin{aligned} \tilde{A}^{q\bar{q}} &= F_q(2 - \beta^2 \sin^2 \Theta) \\ \tilde{C}_{rr}^{q\bar{q}} &= F_q(2 - \beta^2) \sin^2 \Theta \\ \tilde{C}_{nn}^{q\bar{q}} &= -F_q \beta^2 \sin^2 \Theta \\ \tilde{C}_{kk}^{q\bar{q}} &= F_q [2 - (2 - \beta^2) \sin^2 \Theta] \\ \tilde{C}_{rk}^{q\bar{q}} &= \tilde{C}_{kr}^{q\bar{q}} = F_q \sqrt{1 - \beta^2} \sin 2\Theta \\ F_q &= \frac{1}{18} \end{aligned} \quad (45)$$

The resulting $t\bar{t}$ quantum state $\rho^{q\bar{q}}(\beta, \hat{k})$ is entangled in the bulk of the phase space since [57]

$$\Delta^{q\bar{q}} = -C_{nn}^{q\bar{q}} = \frac{\beta^2 \sin^2 \Theta}{2 - \beta^2 \sin^2 \Theta} \geq 0 \quad (46)$$

The above inequality is saturated only at threshold ($\beta = 0$) or for forward production ($\Theta = 0$). In both limits, the $t\bar{t}$ spins are aligned along the beam axis in a maximally correlated but separable mixed state

$$\begin{aligned} C_{ij}^{q\bar{q}}(0, \hat{k}) &= C_{ij}^{q\bar{q}}(\beta, \hat{p}) = \hat{p}_i \hat{p}_j \\ \rho^{q\bar{q}}(0, \hat{k}) &= \rho^{q\bar{q}}(\beta, \hat{p}) = \frac{|\uparrow_{\hat{p}} \uparrow_{\hat{p}}\rangle \langle \uparrow_{\hat{p}} \uparrow_{\hat{p}}| + |\downarrow_{\hat{p}} \downarrow_{\hat{p}}\rangle \langle \downarrow_{\hat{p}} \downarrow_{\hat{p}}|}{2} \end{aligned} \quad (47)$$

where $|\uparrow_{\hat{p}}\rangle, |\downarrow_{\hat{p}}\rangle$ are the spin eigenstates along the direction \hat{p} . This spin alignment at threshold is a consequence of spin conservation, since the $t\bar{t}$ pair is produced from the initial $q\bar{q}$ state via gluon exchange (see Fig. 1), which is a massless spin-1 boson.

Hence, for small production angle or close to threshold, the degree of entanglement is expected to be small, as can be seen in left Fig. 3, where the concurrence of $\rho^{q\bar{q}}(\beta, \hat{k})$ is represented.

In the opposite limit of high transverse momentum p_T (i.e., high energies and production angles close to $\Theta =$

$\pi/2$), the $t\bar{t}$ pair is in a spin-triplet pure state,

$$C_{ij}^{q\bar{q}}(1, \hat{n} \times \hat{p}) = \delta_{ij} - 2\hat{n}_i \hat{n}_j \quad (48)$$

$$\rho^{q\bar{q}}(1, \hat{n} \times \hat{p}) = |\Psi_\infty\rangle \langle \Psi_\infty|, \quad |\Psi_\infty\rangle = \frac{|\uparrow_{\hat{n}} \downarrow_{\hat{n}}\rangle + |\downarrow_{\hat{n}} \uparrow_{\hat{n}}\rangle}{\sqrt{2}}$$

This state is maximally entangled, $C[\rho] = 1$, as seen in upper right corner of left Fig. 3.

With respect to the CHSH inequality, it is also violated by $q\bar{q}$ production in the bulk of phase space. This can be seen in the diagonal basis, where

$$C_+^{q\bar{q}} = 1, \quad C_-^{q\bar{q}} = -C_{nn}^{q\bar{q}} = \Delta^{q\bar{q}} \quad (49)$$

This basis is often called the *off-diagonal* basis [58] in the literature of $q\bar{q}$ production processes, and is commonly used since the $t\bar{t}$ spins along the \hat{u}_+ direction are perfectly correlated. Because of this,

$$\mu^{q\bar{q}}(\beta, \Theta) = [\Delta^{q\bar{q}}(\beta, \Theta)]^2 \geq 0 \quad (50)$$

Remarkably, entanglement and CHSH violation are equivalent conditions for $q\bar{q}$ production.

B. gg production

For gg production, the coefficients of the PM in the helicity basis are

$$\begin{aligned} \tilde{A}^{gg} &= F_g(\beta, \Theta) [1 + 2\beta^2 \sin^2 \Theta - \beta^4(1 + \sin^4 \Theta)] \\ \tilde{C}_{rr}^{gg} &= -F_g(\beta, \Theta) [1 - \beta^2(2 - \beta^2)(1 + \sin^4 \Theta)] \\ \tilde{C}_{nn}^{gg} &= -F_g(\beta, \Theta) [1 - 2\beta^2 + \beta^4(1 + \sin^4 \Theta)] \\ \tilde{C}_{kk}^{gg} &= -F_g(\beta, \Theta) \left[1 - \beta^2 \frac{\sin^2 2\Theta}{2} - \beta^4(1 + \sin^4 \Theta) \right] \\ \tilde{C}_{rk}^{gg} &= \tilde{C}_{kr}^{gg} = F_g(\beta, \Theta) \sqrt{1 - \beta^2} \beta^2 \sin 2\Theta \sin^2 \Theta \\ F_g(\beta, \Theta) &= \frac{7 + 9\beta^2 \cos^2 \Theta}{192(1 - \beta^2 \cos^2 \Theta)^2} \end{aligned} \quad (51)$$

The resulting $t\bar{t}$ quantum state $\rho^{gg}(\beta, \hat{k})$ is entangled iff $\Delta^{gg}(\beta, \Theta) > 0$, where

$$\Delta^{gg} = \frac{\beta^4(1 + \sin^4 \Theta) - \beta^2(1 + \sin^2 \Theta)}{1 + 2\beta^2 \sin^2 \Theta - \beta^4(1 + \sin^4 \Theta)} \quad (52)$$

$$+ \frac{|1 - \beta^2(1 + \sin^2 \Theta)|}{1 + 2\beta^2 \sin^2 \Theta - \beta^4(1 + \sin^4 \Theta)} \quad (53)$$

The second line implies that $\rho^{gg}(\beta, \hat{k})$ is not entangled for $\beta^2(1 + \sin^2 \Theta) = 1$, so there are regions of separability in phase space, in contrast to $q\bar{q}$ production. In particular, two separated regions of entanglement can be distinguished: one close to threshold, and another one for high p_T , delimited by the lower and upper critical boundaries $\beta_{c1}^{\text{PH}}(\Theta), \beta_{c2}^{\text{PH}}(\Theta)$

$$\beta_{c1}^{\text{PH}}(\Theta) = \sqrt{\frac{1 + \sin^2 \Theta - \sqrt{2} \sin \Theta}{1 + \sin^4 \Theta}} \quad (54)$$

$$\beta_{c2}^{\text{PH}}(\Theta) = \frac{1}{(1 + \sin^4 \Theta)^{\frac{1}{4}}} \quad (55)$$

These features can be observed in right Fig. 3, where the concurrence of $\rho^{gg}(M_{t\bar{t}}, \hat{k})$ is represented, with the black solid lines representing the critical boundaries $\beta_{c1,c2}^{\text{PH}}(\Theta)$ between entanglement and separability.

The strong entanglement signature close to threshold results from the fact that the spin polarizations of the gg initial state are allowed to align in different directions. Due to angular momentum conservation, these features produce at threshold a $t\bar{t}$ pair in a spin singlet

$$C_{ij}^{gg}(0, \hat{k}) = -\delta_{ij} \quad (55)$$

$$\rho^{gg}(0, \hat{k}) = |\Psi_0\rangle \langle \Psi_0|, \quad |\Psi_0\rangle = \frac{|\uparrow_{\hat{n}}\downarrow_{\hat{n}}\rangle - |\downarrow_{\hat{n}}\uparrow_{\hat{n}}\rangle}{\sqrt{2}}$$

$$C_{\pm}^{gg} = \frac{-1 + \beta^2(1 + \sin^2 \Theta) \pm \sqrt{\beta^4(1 - 2\sin^2 \Theta + 5\sin^4 \Theta) - 2\beta^6(1 - \sin^2 \Theta + 3\sin^4 \Theta + \sin^6 \Theta) + \beta^8 [1 + \sin^4 \Theta]^2}}{1 + 2\beta^2 \sin^2 \Theta - \beta^4(1 + \sin^4 \Theta)} \quad (56)$$

As a result, an explicit analytical computation of the critical boundaries $\beta_{c1,c2}^{\text{CH}}(\Theta)$ of the regions where the CHSH inequality is violated becomes much more cumbersome; even in the relatively simple case of $\Theta = \pi/2$, the critical values $\beta_{c1,c2}^{\text{CH}}(\pi/2)$ are computed from the zeros of fourth order polynomials in β^2 , finding $\beta_{c1}^{\text{CH}}(\pi/2) \approx 0.367 < \beta_{c1}^{\text{PH}}(\pi/2) = 2^{-1/4} \approx 0.541$ and $\beta_{c2}^{\text{CH}}(\pi/2) \approx 0.931 > \beta_{c2}^{\text{PH}}(\pi/2) = \sqrt{1 - 1/\sqrt{2}} \approx 0.841$.

The numerically computed boundaries $\beta_{c1,c2}^{\text{CH}}(\Theta)$ are represented as black dashed lines in right Fig. 3. As expected, the regions where CHSH inequality is violated are deep inside the entangled regions of phase space, $\beta_{c1}^{\text{CH}}(\Theta) \leq \beta_{c1}^{\text{PH}}(\Theta) \leq \beta_{c2}^{\text{PH}}(\Theta) \leq \beta_{c2}^{\text{CH}}(\Theta)$.

An important conclusion is that the entanglement structure of $t\bar{t}$ production can be mostly understood from basic laws of angular momentum conservation between the initial and final state, without the need to invoke technical details of the specific structure of QCD interactions.

IV. ENTANGLEMENT IN REALISTIC QCD PROCESSES

Because of color confinement, quarks and gluons are not free particles and cannot be found isolated in nature. Instead, they are forming hadrons, which are bound states of quarks through QCD interactions. As a result, we can understand hadrons as a sea of quarks and hadrons, which in this structure are indistinctively denoted as partons [59, 60]. Quantitatively, the composition of a hadron is modeled by its so-called parton distribution function (PDF), which determines the participation of each parton in the momentum transfer of a particular QCD process at a certain energy scale. The PDF describes processes involving the individual partons within

which is maximally entangled.

In the opposite limit of high p_T , gluon fusion produces the same maximally entangled triplet state as $q\bar{q}$ production, Eq. (48). The reason behind this similarity is that for high energies the orbital angular momentum contribution dominates over the spin contribution.

With respect to the violation of the CHSH inequality, the eigenvalues of the correlation matrix are

a global hadron collision. Due to its non-perturbative character, PDF distributions are typically computed by fitting experimental data (see Appendix C for more technical details about PDF). Here, we focus on $t\bar{t}$ production from two main types of hadron processes which are of high relevance for experiments: proton-proton collisions, as in the LHC, and proton-antiproton collisions, as in the Tevatron.

The above considerations modify the results of the previous section as following. For given energy and top direction in the c.m. frame, the PM $R(M_{t\bar{t}}, \hat{k})$ describing the $t\bar{t}$ pair resulting from an hadronic process is computed in terms of each partonic matrix $R^I(M_{t\bar{t}}, \hat{k})$ as

$$R(M_{t\bar{t}}, \hat{k}, \sqrt{s}) = \sum_{I=q\bar{q}, gg} L_I(M_{t\bar{t}}, \sqrt{s}) R^I(M_{t\bar{t}}, \hat{k}) \quad (57)$$

The function $L_I(M_{t\bar{t}}, \sqrt{s})$ is the so-called luminosity function [27], and is computed in terms of the PDF describing the colliding hadrons. The luminosity function can be regarded as the probability distribution of occurrence of each initial state I in the total hadronic process for a given $M_{t\bar{t}}$, depending also on the hadron c.m. energy \sqrt{s} [see Eq. (C2)]. We note that the c.m. frame of the colliding hadrons is not the same as the parton c.m. frame. However, at LO the direction of the parton initial state I in its c.m. frame is to a very good approximation that of the initial hadron beam, so one can take safely \hat{p} along the hadron beam in Fig. 2, which is the one whose direction is controlled in a collider [28].

With the help of the luminosities and the PM, the differential cross-section characterizing $t\bar{t}$ production from

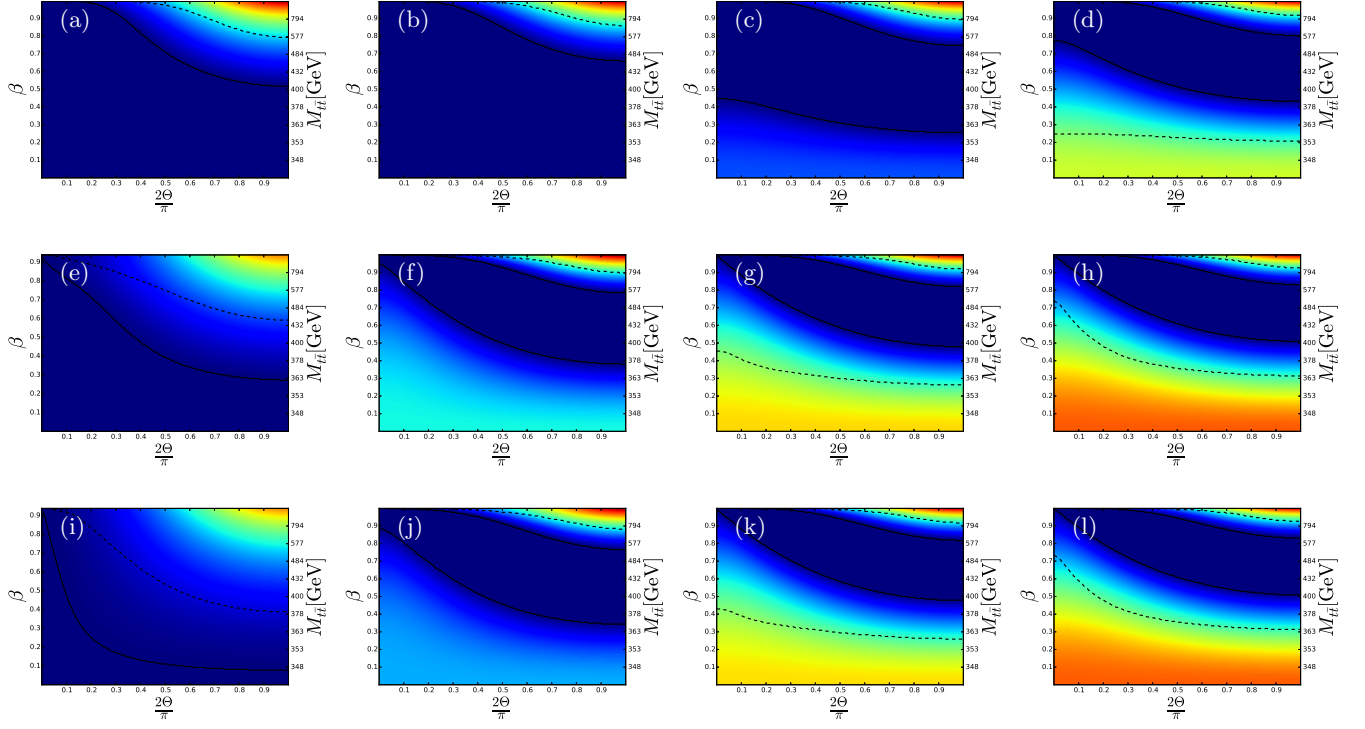


FIG. 4. Same as Fig. 3 but for the quantum state $\rho(M_{t\bar{t}}, \hat{k}, \sqrt{s})$ resulting from realistic hadronic processes. Upper row: Toy model where the probabilities are constant in whole phase space, $w_I(M_{t\bar{t}}, \hat{k}, \sqrt{s}) = w_I$. (a) $w_{gg} = 0.2$. (b) $w_{gg} = 0.4$. (c) $w_{gg} = 0.6$. (d) $w_{gg} = 0.8$. Middle row: $t\bar{t}$ production from pp collisions. (e) $\sqrt{s} = 1$ TeV. (f) $\sqrt{s} = 10$ TeV. (g) $\sqrt{s} = 30$ TeV. (h) $\sqrt{s} = 100$ TeV. Lower row: $t\bar{t}$ production from $p\bar{p}$ collisions. (i)-(l) Same values of \sqrt{s} as (e)-(h), respectively.

a given hadronic process is computed as

$$\begin{aligned} \frac{d\sigma}{d\Omega dM_{t\bar{t}}} &= \frac{\alpha_s^2 \beta}{M_{t\bar{t}}^2} \tilde{A}(M_{t\bar{t}}, \hat{k}, \sqrt{s}) \\ &= \sum_{I=q\bar{q}, gg} L_I(M_{t\bar{t}}, \sqrt{s}) \frac{d\sigma^I}{d\Omega}(M_{t\bar{t}}, \hat{k}) \end{aligned} \quad (58)$$

where the partonic cross-sections σ^I are those of Eq. (40). Thus, the differential cross-section per unit solid angle and per unit c.m. energy at a certain energy $M_{t\bar{t}}$ is just the sum of the partonic differential cross-sections from an initial state I , multiplied by the probability distribution L_I of producing each initial state I with energy $M_{t\bar{t}}$.

Regarding the actual spin quantum state, since $\rho^I = R^I/4\tilde{A}^I$, then

$$\rho(M_{t\bar{t}}, \hat{k}, \sqrt{s}) = \sum_{I=q\bar{q}, gg} w_I(M_{t\bar{t}}, \hat{k}, \sqrt{s}) \rho^I(M_{t\bar{t}}, \hat{k}), \quad (59)$$

Similar expressions can be written for the spin polarizations and spin correlations $\mathbf{B}^\pm(M_{t\bar{t}}, \hat{k}, \sqrt{s})$, $\mathbf{C}(M_{t\bar{t}}, \hat{k}, \sqrt{s})$ of $\rho(M_{t\bar{t}}, \hat{k}, \sqrt{s})$ in terms of their partonic counterparts, computed from Eqs. (45), (51). The weights w_I are obtained from the luminosities as

$$w_I(M_{t\bar{t}}, \hat{k}, \sqrt{s}) = \frac{L_I(M_{t\bar{t}}, \sqrt{s}) \tilde{A}^I(M_{t\bar{t}}, \hat{k})}{\sum_J L_J(M_{t\bar{t}}, \sqrt{s}) \tilde{A}^J(M_{t\bar{t}}, \hat{k})}. \quad (60)$$

and represent the probability of production of each individual partonic quantum state $\rho^I(M_{t\bar{t}}, \hat{k})$ in the total mix, satisfying $w_{q\bar{q}} + w_{gg} = 1$. They can be simply understood as the probability of occurrence of the initial state I , L_I , multiplied by the probability of producing a $t\bar{t}$ pair from I , proportional to the coefficient $\tilde{A}^I(M_{t\bar{t}}, \hat{k})$.

We stress that the specific physics of the particular hadron collision only enters in the calculations through the probabilities $w_I(M_{t\bar{t}}, \hat{k}, \sqrt{s})$, which are PDF dependent. Hence, the LO QCD processes $q\bar{q}$ and gg are the building blocks of any realistic hadronic production process, whose specific nature is reduced to change the amount of mixing between them. From a more general perspective, we can regard the production spin density matrices $R^I(M_{t\bar{t}}, \hat{k})$ and the luminosities $L_I(M_{t\bar{t}}, \sqrt{s})$ as inputs from the theory of high-energy physics, from which we can compute the physical spin density matrices $\rho^I(M_{t\bar{t}}, \hat{k})$ and the probabilities $w_I(M_{t\bar{t}}, \hat{k}, \sqrt{s})$. Once done, we are simply left with a typical problem in quantum information involving two-qubit quantum states and a statistical incoherent mixture between them, where the usual techniques of the field can be applied.

In order to understand better how the mixture between $q\bar{q}$ and gg initial states affects the $t\bar{t}$ quantum state $\rho(M_{t\bar{t}}, \hat{k}, \sqrt{s})$, we first use a toy model where both partonic probabilities are constant, $w_I(M_{t\bar{t}}, \hat{k}, \sqrt{s}) = w_I$.

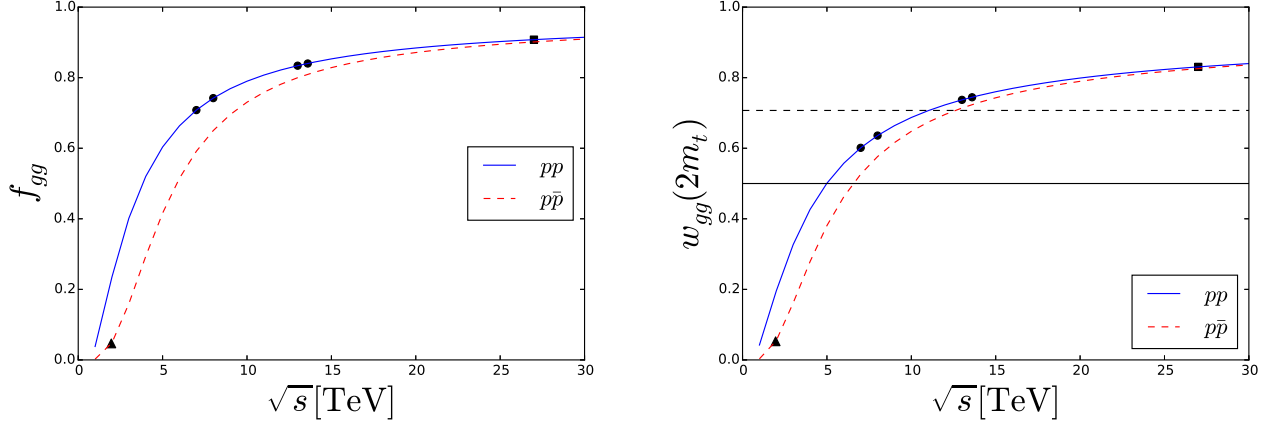


FIG. 5. Study of the dependence of $t\bar{t}$ production mechanism with the c.m. energy \sqrt{s} for pp collisions (solid blue line) and for $p\bar{p}$ collisions (dashed red line), corresponding to the LHC and Tevatron, respectively. Black markers indicate the values for c.m. energies of actual high-energy colliders. Circles: Run 1 ($\sqrt{s} = 7, 8$ TeV), Run 2 ($\sqrt{s} = 13$ TeV) and Run 3 ($\sqrt{s} = 13.6$ TeV) of LHC. Squares: Possible upgrade of the LHC ($\sqrt{s} = 27$ TeV). Triangles: Tevatron ($\sqrt{s} = 1.96$ TeV). Left: Gluon fraction f_{gg} . Right: gg probability at threshold $w_{gg}(2m_t)$. Horizontal lines mark the critical values $w_{gg,c} = 1/2$ for entanglement (solid) and $w_{gg,CH,c} = 1/\sqrt{2}$ for CHSH violation (dashed).

We gradually introduce gg production in a pure $q\bar{q}$ process in upper row of Fig. 4. For a small amount of gg processes, the effect of mixing is reduced to shrink the entangled region towards the high p_T region. By further increasing the amount of gg processes in the mix, at some point entangled $t\bar{t}$ states also emerge at threshold. We can actually compute the critical value w_c^{PH} at which entanglement appears from Eq. (42), which at threshold reads for the total hadronic process as

$$\Delta(\beta = 0, \Theta) = \frac{w_{gg} + |3w_{gg} - 1| - 1}{2} \quad (61)$$

For $w_{gg} > 1/3$, $\Delta(0, \Theta) = 2w_{gg} - 1$, which simply gives

$$w_c^{\text{PH}} = \frac{1}{2} \quad (62)$$

Hence, in order to have entanglement close to threshold, we need that at least 50% of the $t\bar{t}$ pairs are produced through gluon fusion. Regarding the violation of the CHSH inequality, the corresponding critical value w_c^{CH} is computed by switching to the off-diagonal basis where both correlation matrices are diagonalized [ρ^{gg} at threshold is a spin singlet, invariant under rotations; see also Eq. (55)]. This gives

$$\mu(\beta = 0, \Theta) = 2w_{gg}^2 - 1 \quad (63)$$

from where we find

$$w_c^{\text{CH}} = \frac{1}{\sqrt{2}} > w_c^{\text{PH}} \quad (64)$$

Once this simple model is understood, we switch to real hadron processes. We analyze $t\bar{t}$ production from

pp collisions for different c.m. energies in central row of Fig. 4. By direct comparison with upper row, we observe that for low c.m. energies $q\bar{q}$ processes dominate. However, the amount of gg processes increases with the c.m. energy, eventually dominating the $t\bar{t}$ production mechanism. A similar calculation is shown in the lower row of Fig. 4 for $p\bar{p}$ collisions where, although $q\bar{q}$ contributions are stronger at low energies, gg dominance is again recovered for sufficiently high c.m. energies and both processes seem to converge to a similar quantum state.

We can further quantify the amount of mixing of $q\bar{q}$ and gg processes in the total $t\bar{t}$ production by computing the relative fraction of each contribution to the total cross-section from Eq. (58):

$$f_I \equiv \frac{\frac{\sqrt{s}}{2m_t} \int dM_{t\bar{t}} \int d\Omega L_I \frac{d\sigma^I}{d\Omega}}{\frac{\sqrt{s}}{2m_t} \int dM_{t\bar{t}} \int d\Omega \frac{d\sigma}{d\Omega dM_{t\bar{t}}}} \quad (65)$$

where we remark that the maximum invariant mass $M_{t\bar{t}}$ achievable by the $t\bar{t}$ pair is precisely the c.m. energy of the hadron pair, $M_{t\bar{t}} = \sqrt{s}$. The fraction of gg processes f_{gg} for both pp and $p\bar{p}$ collisions is represented in left Fig. 5, where its predicted increase with the c.m. energy suggested by the entanglement analysis is clearly observed, as well as the stronger contribution of $q\bar{q}$ processes for $p\bar{p}$ collisions with respect to pp at low energies. In particular, at high energies, both hadronic processes converge to the same gluon fraction f_{gg} . This analysis suggests that entanglement measurements can be also used to understand the underlying structure of a certain high-energy process without direct knowledge of it.

A related plot is that of right Fig. 5, in which the threshold values of the gluon probability $w_{gg}(2m_t, \sqrt{s})$ are represented (there is no angular dependence at threshold). We observe that entanglement [$w_{gg}(2m_t, \sqrt{s}) > w_c^{\text{PH}} = 1/2$] can be achieved in pp collisions for small c.m. energies $\sqrt{s} \gtrsim 5$ TeV, below current LHC energies. In particular, the relevant experimental values $\sqrt{s} = 7, 8$ TeV [35–37], $\sqrt{s} = 13$ TeV [38, 39] and $\sqrt{s} = 13.6$ TeV are marked by circles, corresponding to the c.m. energies of Run 1, Run 2 and the oncoming Run 3 of LHC, respectively. The expected value for a possible upgrade of the LHC is $\sqrt{s} = 27$ TeV [61], marked by a square. With respect to CHSH violation [$w_{gg}(2m_t, \sqrt{s}) > w_c^{\text{CH}} = 1/\sqrt{2}$], we observe that we need larger energies $\sqrt{s} \gtrsim 10$ TeV, and even Run 2 and Run 3 c.m. energies are slightly above this limit. For $p\bar{p}$ collisions, even threshold entanglement cannot be observed since the c.m. energies required are well above the maximum energy ever achieved at the Tevatron, $\sqrt{s} = 1.96$ TeV [32–34], marked by a triangle.

Therefore, the Tevatron and the LHC provide experimental realizations to a very good approximation of the two main paradigms of $t\bar{t}$ QCD production, $q\bar{q}$ and gg interactions, respectively. Finally, we note that the c.m. energy for pp collisions in the Future Circular Collider (FCC), $\sqrt{s} = 100$ TeV [62], is represented explicitly in Fig. 4h.

V. EXPERIMENTAL OBSERVABLES

A. Experimental motivation

How are all these spin magnitudes translated into actual observables that can be measured in high-energy colliders? This is where the unique properties of the top quark enter in place. As explained in the Introduction, the top quark is the most massive particle of the Standard Model. This property makes that even its large width $\Gamma_t \simeq 1$ GeV is still narrow when compared to its huge mass $m_t \simeq 173$ GeV. In turn, this large width results in a very short lifetime $\tau = 1/\Gamma_t \sim 10^{-25}$ s. This implies that a $t\bar{t}$ pair decays so fast that any other process such as hadronisation (with a time scale $\sim 10^{-23}$ s) or spin decorrelation (with a time scale $\sim 10^{-21}$ s) cannot affect their spins, which are directly translated into the properties of the decay products. This is what makes the top quark so special, as any other quark hadronizes before decaying, losing its spin information in the process. On the other hand, if the top quark did not decay, its spin state could not be extracted because detectors only measure the momentum of the arriving particles.

Quantitatively, we describe the decay of a top quark to some final state F in terms of a decay spin density matrix, defined in the top rest frame as

$$\Gamma_{\alpha'\alpha}^F = \langle F | T | t\alpha \rangle \langle t\alpha' | T^\dagger | F \rangle \quad (66)$$

where $|t\alpha\rangle$ is the top quantum state with zero momentum

and spin α , $|F\rangle$ is the final state after the decay, and T is here the *on-shell* T -matrix describing the amplitude of the decay process. A similar decay spin density matrix $\bar{\Gamma}_{\beta'\beta}^{\bar{F}}$ can be defined for the decay of an antitop quark to a final state \bar{F} .

The idea is to describe the production and decay of a $t\bar{t}$ pair using the production and decay spin density matrices. Specifically, we consider a $t\bar{t}$ pair with fixed c.m. energy and momentum produced in a hadron collision, whose quantum state is described by a PM $R(M_{t\bar{t}}, \hat{k}, \sqrt{s})$. In the so-called narrow width approximation, valid since $\Gamma_t \ll m_t$ [25], the differential cross-section characterizing the decay of a $t\bar{t}$ pair to two final states $F\bar{F}$ is proportional to

$$\begin{aligned} d\sigma &\sim \sum_{\alpha\alpha',\beta\beta'} R_{\alpha\beta,\alpha'\beta'}(M_{t\bar{t}}, \hat{k}, \sqrt{s}) \Gamma_{\alpha'\alpha}^F \bar{\Gamma}_{\beta'\beta}^{\bar{F}} \quad (67) \\ &= \text{tr} \left[\left(\Gamma^F \otimes \bar{\Gamma}^{\bar{F}} \right) R(M_{t\bar{t}}, \hat{k}, \sqrt{s}) \right] \end{aligned}$$

Thus, the information about the quantum state of the $t\bar{t}$ pair, encoded in $R(M_{t\bar{t}}, \hat{k}, \sqrt{s})$, is contained in the cross-section characterizing the decay products of the final states $F\bar{F}$.

We can retrieve this information by considering final states containing a lepton ℓ , which can be either an electron or a muon, $\ell = e, \mu$. In particular, we consider the electroweak leptonic decay of both the top and the antitop quark

$$\begin{aligned} t \rightarrow b + W^+ &\rightarrow b + \ell^+ + \nu_\ell, \\ \bar{t} \rightarrow \bar{b} + W^- &\rightarrow \bar{b} + \ell^- + \bar{\nu}_\ell \end{aligned} \quad (68)$$

where $F = b\ell^+\nu_\ell$, with ℓ^+ the antilepton and ν_ℓ its associated neutrino, and \bar{F} its conjugate, $\bar{F} = \bar{b}\ell^-\bar{\nu}_\ell$. A diagrammatic representation of the top/antitop decay is provided in Fig. 6.

The expression for the decay spin density matrices vastly simplifies if we integrate out all the degrees of freedom of the final states $F\bar{F}$ except for the lepton directions. In that case, due to rotational invariance in the top (antitop) rest frames, the resulting decay spin density matrices $\Gamma_\ell, \bar{\Gamma}_\ell$ can only be of the form [30]

$$\Gamma_\ell \propto \frac{I_2 + \kappa_\ell(\hat{\ell}_+ \cdot \sigma)}{2}, \quad \bar{\Gamma}_\ell = \frac{I_2 + \bar{\kappa}_\ell(\hat{\ell}_- \cdot \sigma)}{2} \quad (69)$$

$\hat{\ell}_\pm$ being the antilepton (lepton) directions in each one of the parent top (antitop) rest frames and $\kappa_\ell = -\bar{\kappa}_\ell \simeq 1$ are the so-called spin analyzing powers of leptons.

As a result, the cross-section $\sigma_{\ell\bar{\ell}}$ characterizing the $\ell^+\ell^-$ angular distribution reads

$$\begin{aligned} \frac{d\sigma_{\ell\bar{\ell}}}{d\Omega_+ d\Omega_- dM_{t\bar{t}} d\Omega_{\hat{k}}} &\propto \frac{\alpha_s^2 \beta}{M_{t\bar{t}}^2} \text{tr} \left[(\Gamma_\ell \otimes \bar{\Gamma}_\ell) R(M_{t\bar{t}}, \hat{k}, \sqrt{s}) \right] \\ &= \frac{\alpha_s^2 \beta}{M_{t\bar{t}}^2} \left[\tilde{A} + \tilde{\mathbf{B}}^+ \cdot \hat{\ell}_+ - \tilde{\mathbf{B}}^- \cdot \hat{\ell}_- - \hat{\ell}_+ \cdot \tilde{\mathbf{C}} \cdot \hat{\ell}_- \right] \end{aligned} \quad (70)$$

where Ω_{\pm} are the solid angles associated to $\hat{\ell}_{\pm}$, and $\Omega_{\hat{k}}$ that associated to the c.m. top direction \hat{k} . The differential elements $dM_{t\bar{t}}d\Omega_{\hat{k}}$ arise because we are considering the decay of a $t\bar{t}$ pair with fixed energy and direction. The total angular differential cross section describing the leptons arising from $t\bar{t}$ decay is then obtained by integration over all possible top directions and c.m. energies:

$$\frac{d\sigma_{\ell\bar{\ell}}}{d\Omega_+ d\Omega_-} = \int_{2m_t}^{\sqrt{s}} dM_{t\bar{t}} \int d\Omega \frac{d\sigma_{\ell\bar{\ell}}}{d\Omega_+ d\Omega_- dM_{t\bar{t}} d\Omega_{\hat{k}}} \quad (71)$$

This implies that the normalized angular differential cross-section characterizing the dileptonic decay is

$$\frac{1}{\sigma_{\ell\bar{\ell}}} \frac{d\sigma_{\ell\bar{\ell}}}{d\Omega_+ d\Omega_-} = \frac{1 + \mathbf{B}^+ \cdot \hat{\ell}_+ - \mathbf{B}^- \cdot \hat{\ell}_- - \hat{\ell}_+ \cdot \mathbf{C} \cdot \hat{\ell}_-}{(4\pi)^2} \quad (72)$$

where the vectors \mathbf{B}^{\pm} and the matrix \mathbf{C} are the integrated values of the top/antitop spin polarizations and the spin correlation matrix, respectively. This implies that we can measure all the integrated spin information of a $t\bar{t}$ pair by fitting the differential cross-section of the leptonic decay products.

In particular, from the kinematic reconstruction of each event, the momentum of the $t\bar{t}$ and $\ell^+\ell^-$ pairs can be determined. By defining the polar angle around a certain direction given by the unit vector \hat{u}_i , $\cos\theta_{\pm}^i \equiv \hat{\ell}_{\pm} \cdot \hat{u}_i$, and after integrating over the azimuthal angles, we find that the spin polarizations can be easily obtained from a linear fit of the angular distributions for each individual lepton as

$$\frac{1}{\sigma_{\ell\bar{\ell}}} \frac{d\sigma_{\ell\bar{\ell}}}{d\cos\theta_{\pm}^i} = \frac{1}{2} (1 \pm B_i^{\pm} \cos\theta_{\pm}^i) \quad (73)$$

The spin correlations between two directions i, j can be measured from the distribution of the product $x_{ij} \equiv \cos\theta_+^i \cos\theta_-^j$, obtained from integration of Eq. (72),

$$\frac{1}{\sigma_{\ell\bar{\ell}}} \frac{d\sigma_{\ell\bar{\ell}}}{dx_{ij}} = \frac{1}{2} [1 - C_{ij} x_{ij}] \ln \frac{1}{|x_{ij}|} \quad (74)$$

Another measurable magnitude of interest is the trace of the correlation matrix, which can be directly obtained from

$$\frac{1}{\sigma_{\ell\bar{\ell}}} \frac{d\sigma_{\ell\bar{\ell}}}{d\cos\varphi} = \frac{1}{2} (1 - D \cos\varphi), \quad D = \frac{\text{tr}[\mathbf{C}]}{3} \quad (75)$$

where φ is the angle between the lepton directions in each one of their parent top and antitop rest frames, $\cos\varphi = \hat{\ell}_+ \cdot \hat{\ell}_-$.

The determination of the momentum of the $t\bar{t}$ pair also implies that the spin polarizations and correlations can be obtained in any orthonormal basis, in particular in the helicity basis considered so far. The measurement of the $t\bar{t}$ spin polarizations and spin correlations through this technique is well-established, and has already been

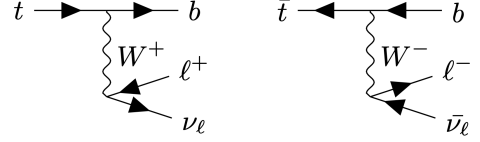


FIG. 6. Representative Feynman diagrams for a leptonic electroweak decay of a top (left) and antitop (right) quark.

performed by the CMS collaboration at the LHC [38], where \mathbf{B}^{\pm} , \mathbf{C} were obtained in the helicity basis, with no restrictions on $t\bar{t}$ phase space. However, no entanglement signature was provided by these measurements.

B. Integrated expectation values

The formalism of the previous subsection focused on integrated values over all the $(M_{t\bar{t}}, \hat{k})$ phase space. However, as explained, the $t\bar{t}$ momenta can be experimentally reconstructed, allowing to restrict the contributions to the integral of Eq. (70) to specific regions Π of the $t\bar{t}$ phase space. In that case, the measured spin polarizations and spin correlations would correspond to integrated values just within the region Π . This allows to further explore the $t\bar{t}$ properties in search of richer physics. For instance, we can take Π within the regions of phase space where entanglement is present (delimited by the black lines in Figs. 3, 4).

Ideally, one would restrict Π to a small bin around a given value $(M_{t\bar{t}}, \hat{k})$, which would allow to study the individual spin quantum states $\rho(M_{t\bar{t}}, \hat{k}, \sqrt{s})$. However, in actual experiments, the signal needs to be integrated in order to collect sufficient number of events for achieving statistically significant measurements. Therefore, an adaptation of the formalism developed in the previous sections is required.

We begin by noting that the total quantum state describing the $t\bar{t}$ pairs from a certain hadronic process is obtained by generalizing Eq. (38) as

$$\rho_T(\sqrt{s}) = \frac{1}{\sigma} \sum_{\alpha\beta, \alpha'\beta'} \int_{2m_t}^{\sqrt{s}} dM_{t\bar{t}} \int d\Omega \frac{d\sigma}{d\Omega dM_{t\bar{t}}} \times \rho_{\alpha\beta, \alpha'\beta'}(M_{t\bar{t}}, \hat{k}, \sqrt{s}) \frac{|M_{t\bar{t}} \hat{k} \alpha \beta \rangle \langle M_{t\bar{t}} \hat{k} \alpha' \beta'|}{\langle M_{t\bar{t}} \hat{k} | M_{t\bar{t}} \hat{k} \rangle} \quad (76)$$

If we consider now some observable O , diagonal in momentum space, with matrix elements $O_{\alpha'\beta', \alpha\beta}(M_{t\bar{t}}, \hat{k}) = \langle M_{t\bar{t}} \hat{k} \alpha' \beta' | O | M_{t\bar{t}} \hat{k} \alpha \beta \rangle / \langle M_{t\bar{t}} \hat{k} | M_{t\bar{t}} \hat{k} \rangle$, its expectation value $\langle O \rangle = \text{tr}[O \rho_T(\sqrt{s})]$ is simply computed as

$$\langle O \rangle = \frac{1}{\sigma} \int_{2m_t}^{\sqrt{s}} dM_{t\bar{t}} \int d\Omega \frac{d\sigma}{d\Omega dM_{t\bar{t}}} \text{tr} [O(M_{t\bar{t}}, \hat{k}) \rho(M_{t\bar{t}}, \hat{k}, \sqrt{s})] \quad (77)$$

This expectation value is readily understood as the average of the expectation values of O for all possible quantum states $\rho(M_{t\bar{t}}, \hat{k}, \sqrt{s})$ of the $t\bar{t}$ pair, with a probability proportional to the differential cross-section of the process, everything normalized by the total cross section for $t\bar{t}$ production.

The above equation can be simply rewritten in terms of the PM as

$$\langle O \rangle = \frac{\int_{2m_t}^{\sqrt{s}} dM_{t\bar{t}} \int d\Omega \frac{\alpha_s^2 \beta}{M_{t\bar{t}}^2} \text{tr} [O(M_{t\bar{t}}, \hat{k}) R(M_{t\bar{t}}, \hat{k}, \sqrt{s})]}{\int_{2m_t}^{\sqrt{s}} dM_{t\bar{t}} \int d\Omega \frac{\alpha_s^2 \beta}{M_{t\bar{t}}^2} \text{tr} [R(M_{t\bar{t}}, \hat{k}, \sqrt{s})]} \quad (78)$$

From these considerations, it is immediate to compute the reduced quantum state $\rho_{\text{TP}}(\sqrt{s})$ that describes the $t\bar{t}$ quantum state within a certain region Π of phase space by projecting only onto the relevant states $|M_{t\bar{t}}\hat{k}\rangle$ contained in Π :

$$\rho_{\text{TP}}(\sqrt{s}) = \frac{1}{\sigma_{\Pi}} \sum_{\alpha\beta, \alpha'\beta'} \int_{\Pi} d\Omega dM_{t\bar{t}} \frac{d\sigma}{d\Omega dM_{t\bar{t}}} \times \rho_{\alpha\beta, \alpha'\beta'}(M_{t\bar{t}}, \hat{k}, \sqrt{s}) \frac{|M_{t\bar{t}}\hat{k}\alpha\beta\rangle \langle M_{t\bar{t}}\hat{k}\alpha'\beta'|}{\langle M_{t\bar{t}}\hat{k}|M_{t\bar{t}}\hat{k}\rangle} \quad (79)$$

with the partition function σ_{Π} being the $t\bar{t}$ cross-section in the region Π

$$\sigma_{\Pi} \equiv \int_{\Pi} d\Omega dM_{t\bar{t}} \frac{d\sigma}{d\Omega dM_{t\bar{t}}} \quad (80)$$

Similar equations can be obtained for the expectation value $\langle O \rangle_{\Pi}$ of any observable O in the region Π by cutting the integrals of Eqs. (77), (78) to the region Π .

Furthermore, we can define a genuine two-qubit quantum state by taking the trace in momentum space

$$\rho_{\Pi}(\sqrt{s}) \equiv \text{tr}_{M_{t\bar{t}}\hat{k}} [\rho_{\text{TP}}(\sqrt{s})] = \sum_{\alpha\beta, \alpha'\beta'} \rho_{\Pi, \alpha\beta, \alpha'\beta'} |\alpha\beta\rangle \langle \alpha'\beta'| \quad (81)$$

In matrix notation,

$$\begin{aligned} \rho_{\Pi}(\sqrt{s}) &= \frac{1}{\sigma_{\Pi}} \int_{\Pi} d\Omega dM_{t\bar{t}} \frac{d\sigma}{d\Omega dM_{t\bar{t}}} \rho(M_{t\bar{t}}, \hat{k}, \sqrt{s}) \\ &= \frac{\sum_I \int_{\Pi} d\Omega dM_{t\bar{t}} \frac{\alpha_s^2 \beta}{M_{t\bar{t}}^2} L_I(M_{t\bar{t}}, \sqrt{s}) R^I(M_{t\bar{t}}, \hat{k})}{\sum_I \int_{\Pi} d\Omega dM_{t\bar{t}} \frac{\alpha_s^2 \beta}{M_{t\bar{t}}^2} L_I(M_{t\bar{t}}, \sqrt{s}) 4\tilde{A}^I(M_{t\bar{t}}, \hat{k})} \end{aligned} \quad (82)$$

As a two-qubit quantum state, ρ_{Π} is determined by the respective integrated spin polarizations and spin correlations $\mathbf{B}_{\Pi}^{\pm}, \mathbf{C}_{\Pi}$, which can be measured from the cross-section of the dileptonic decay, Eqs. (73), (74). However, since ρ_{Π} is already the result of an integration in phase space, the orthonormal basis used to compute $\mathbf{B}_{\Pi}^{\pm}, \mathbf{C}_{\Pi}$ cannot depend on $(M_{t\bar{t}}, \hat{k})$, which invalidates the use of the helicity or the diagonal basis. A natural choice is then the beam basis [28] $\{\hat{x}, \hat{y}, \hat{z}\}$, where $\hat{z} = \hat{p}$ points

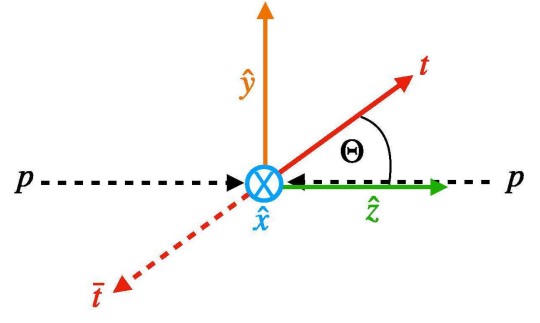


FIG. 7. Orthonormal beam basis, defined in the c.m. frame. The \hat{z} vector points along the direction of the initial hadron beam, $\hat{z} = \hat{p}$, while \hat{x}, \hat{y} point fixed transverse directions.

along the initial state beam and \hat{x}, \hat{y} point transverse directions to the beam, where all directions are determined in the c.m. frame. The beam basis is represented in right Fig. 7.

The upshot of the discussion of this subsection is that we can aim at obtaining entanglement signatures by measuring integrated values of the entanglement criteria in selected regions Π of phase space where the $t\bar{t}$ pair is expected to be entangled. Moreover, we can analyze directly if the integrated two-qubit quantum state ρ_{Π} is entangled. In fact, by measuring the coefficients $\mathbf{B}_{\Pi}^{\pm}, \mathbf{C}_{\Pi}$ we can perform the full quantum tomography of ρ_{Π} .

Due to its experimental simplicity and availability of analytical results, leading to a better understanding of the physics involved, in the following we take the region Π as $\Pi = \Sigma \times S^2$, that is, we integrate over all possible top directions so we only have to specify the cuts in the invariant mass spectrum delimiting the regions Σ .

C. Angular integration

We compute first the distributions and correlations resulting from averaging over the angular coordinates. We start with the PM for each partonic initial state I :

$$R_{\Omega}^I(M_{t\bar{t}}) = \frac{1}{4\pi} \int d\Omega R^I(M_{t\bar{t}}, \hat{k}) \quad (83)$$

The invariance under rotations around the beam axis implies that, in the beam basis, the correlation matrix describing $R_{\Omega}^I(M_{t\bar{t}})$ after azimuthal integration is diagonal, $\tilde{C}_{ij}^I = \delta_{ij} \tilde{C}_j^I$, with $\tilde{C}_x^I = \tilde{C}_y^I \equiv \tilde{C}_{\perp}^I$. Thus, the matrices $R_{\Omega}^I(M_{t\bar{t}})$ are characterized by just 3 parameters that can be computed analytically from Eqs. (45), (51): $\tilde{A}^I(M_{t\bar{t}})$, $\tilde{C}_{\perp}^I(M_{t\bar{t}})$ and $\tilde{C}_z^I(M_{t\bar{t}})$, where $\tilde{A}^I(M_{t\bar{t}})$ is simply the angular average of $\tilde{A}^I(M_{t\bar{t}}, \hat{k})$. Actual spin density matrices $\rho_{\Omega}^I(M_{t\bar{t}})$ are obtained from $R_{\Omega}^I(M_{t\bar{t}})$ by normalization, $\rho_{\Omega}^I(M_{t\bar{t}}) = R_{\Omega}^I(M_{t\bar{t}})/4\tilde{A}^I(M_{t\bar{t}})$.

With respect to entanglement, due to the symmetry around the beam axis of ρ_{Ω}^I , the Peres-Horodecki criterion is equivalent now to $\delta_{\perp}^I > 0$ [see Eq. (B16) and

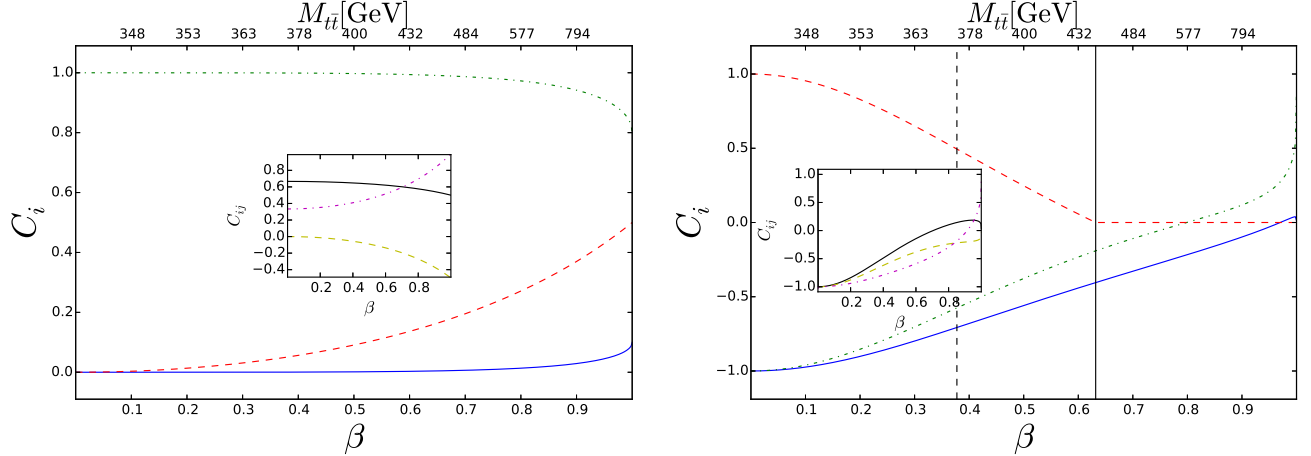


FIG. 8. Angular averaged spin correlations as a function of β . Main plot shows C_{\perp}^I (solid blue) and C_z^I (dashed-dotted green). Inset shows C_{rr}^I (solid black), C_{nn}^I (dashed yellow), and C_{kk}^I (dashed-dotted purple). Left: $I = q\bar{q}$. Dashed red line is $\Delta_{\Omega}^{q\bar{q}}$. Right: $I = gg$. Dashed red line is $C[\rho_{\Omega}^{gg}] = \max(\delta_{\Omega}^{gg}, 0)$. Vertical lines represent the critical values β_c^{CH} (dashed) and β_c^{PH} (solid), above which there is no CHSH violation and entanglement, respectively.

ensuing discussion], with

$$\delta_{\Omega}^I \equiv \frac{-C_z^I + |2C_{\perp}^I| - 1}{2} \quad (84)$$

from where the concurrence reads $C[\rho_{\Omega}^I] = \max(\delta_{\Omega}^I, 0)$.

Regarding the CHSH violation, ρ_{Ω}^I can achieve it iff $\mu_{\Omega}^I > 0$, where now

$$\mu_{\Omega}^I(M_{t\bar{t}}) \equiv 2C_{\perp}^{I2} + C_z^{I2} - \min\{C_{\perp}^{I2}, C_z^{I2}\} - 1 \quad (85)$$

It is also useful to compute the angular average of the expectation values of the spin correlations in the helicity and the diagonal basis, which are computed similarly as

$$C_{ij}^I(M_{t\bar{t}}) = \frac{\tilde{C}_{ij}^I(M_{t\bar{t}})}{\tilde{A}^I(M_{t\bar{t}})}, \quad \tilde{C}_{ij}^I(M_{t\bar{t}}) \equiv \frac{1}{4\pi} \int d\Omega \tilde{C}_{ij}^I(M_{t\bar{t}}, \hat{k}) \quad (86)$$

We note that the matrix $\tilde{C}_{ij}^I(M_{t\bar{t}})$ is also diagonal in the helicity basis after the angular averaging since $\tilde{C}_{kr}^I(M_{t\bar{t}})$ vanishes at LO due to its odd parity under inversion.

Indeed, a complementary entanglement signature can be obtained from the angular average of Δ^I ,

$$\Delta_{\Omega}^I(M_{t\bar{t}}) \equiv \frac{-C_{nn}^I(M_{t\bar{t}}) + |C_{kk}^I(M_{t\bar{t}}) + C_{rr}^I(M_{t\bar{t}})| - 1}{2} \quad (87)$$

This is because if all substates $\rho^I(M_{t\bar{t}}, \hat{k})$ for fixed $M_{t\bar{t}}$ were separable, $\Delta^I(M_{t\bar{t}}, \hat{k}) \leq 0$ and thus $\Delta_{\Omega}^I(M_{t\bar{t}}) \leq 0$. Hence, $\Delta_{\Omega}^I(M_{t\bar{t}}) > 0$ necessarily implies that some of the substates within $\rho^I(M_{t\bar{t}}, \hat{k})$ must be entangled. The details about the analytical calculation of the angular integrals involved in these calculations are provided in Appendix D.

1. $q\bar{q}$ production

We obtain for $R_{\Omega}^{q\bar{q}}(M_{t\bar{t}})$ that

$$\begin{aligned} \tilde{A}^{q\bar{q}}(M_{t\bar{t}}) &= \frac{1}{9} \left[1 - \frac{\beta^2}{3} \right], \\ \tilde{C}_{\perp}^{q\bar{q}}(M_{t\bar{t}}) &= \frac{2}{135} f(\beta) \\ \tilde{C}_z^{q\bar{q}}(M_{t\bar{t}}) &= \frac{1}{9} \left[1 - \frac{\beta^2}{3} - \frac{4}{15} f(\beta) \right] \\ f(\beta) &\equiv \frac{\left(1 - \sqrt{1 - \beta^2} \right)^2}{2} \end{aligned} \quad (88)$$

while for the angular averages of the helicity spin correlations we find

$$\begin{aligned} \tilde{C}_{rr}^{q\bar{q}}(M_{t\bar{t}}) &= \frac{(2 - \beta^2)}{27} \\ \tilde{C}_{nn}^{q\bar{q}}(M_{t\bar{t}}) &= -\frac{\beta^2}{27} \\ \tilde{C}_{kk}^{q\bar{q}}(M_{t\bar{t}}) &= \frac{1 + \beta^2}{27} \end{aligned} \quad (89)$$

These results imply that the quantum state $\rho_{\Omega}^{q\bar{q}}$ is completely separable as

$$\delta_{\Omega}^{q\bar{q}}(M_{t\bar{t}}) = \frac{-1 + \frac{\beta^2}{3} + \frac{4}{15} f(\beta)}{1 - \frac{\beta^2}{3}} < 0 \quad (90)$$

We stress that this only means that the angular averaged state $\rho_{\Omega}^{q\bar{q}}$ so defined is separable, but not that entanglement cannot be detected after the angular average. Indeed,

$$\Delta_{\Omega}^{q\bar{q}}(M_{t\bar{t}}) = \frac{\beta^2}{3 - \beta^2} \geq 0 \quad (91)$$

which means that entanglement can be detected in the whole energy range (except exactly at threshold, $\beta = 0$).

Left Fig. 8 displays all the angular averaged magni-

tudes for $I = q\bar{q}$.

2. gg production

We obtain for $R^{gg}(M_{t\bar{t}})$ that

$$\begin{aligned}\tilde{A}^{gg}(M_{t\bar{t}}) &= \frac{1}{192} \left[-59 + 31\beta^2 + (66 - 36\beta^2 + 2\beta^4) \frac{\operatorname{atanh}(\beta)}{\beta} \right] \\ \tilde{C}_{\perp}^{gg}(M_{t\bar{t}}) &= \frac{1 - \beta^2}{192} \left[9 - 16 \frac{\operatorname{atanh}(\beta)}{\beta} \right] + g(\beta) \\ \tilde{C}_z^{gg}(M_{t\bar{t}}) &= \frac{1}{192} \left[-109 + 49\beta^2 + (102 - 72\beta^2 + 2\beta^4) \frac{\operatorname{atanh}(\beta)}{\beta} \right] - 2g(\beta) \\ g(\beta) &\equiv \frac{f(\beta)}{96\beta^4} \left[49 - \frac{149}{3}\beta^2 + \frac{24}{5}\beta^4 - (49 - 66\beta^2 + 17\beta^4) \frac{\operatorname{atanh}(\beta)}{\beta} \right]\end{aligned}\tag{92}$$

while for the helicity spin correlations we find

$$\begin{aligned}\tilde{C}_{rr}^{gg}(M_{t\bar{t}}) &= -\frac{1}{192} \left[87 - 31\beta^2 + 66 \frac{\frac{\operatorname{atanh}(\beta)}{\beta} - 1}{\beta^2} - (102 - 38\beta^2 + 2\beta^4) \frac{\operatorname{atanh}(\beta)}{\beta} \right] \\ \tilde{C}_{nn}^{gg}(M_{t\bar{t}}) &= -\frac{1}{192} \left[41 - 31\beta^2 - (34 - 36\beta^2 + 2\beta^4) \frac{\operatorname{atanh}(\beta)}{\beta} \right] \\ \tilde{C}_{kk}^{gg}(M_{t\bar{t}}) &= -\frac{1}{192} \left[-37 + 31\beta^2 - 66 \frac{\frac{\operatorname{atanh}(\beta)}{\beta} - 1}{\beta^2} + (66 - 34\beta^2 + 2\beta^4) \frac{\operatorname{atanh}(\beta)}{\beta} \right]\end{aligned}\tag{93}$$

We note that $C_{\perp}^{gg}(M_{t\bar{t}}) < 0$ for all the energies of interest (the sign crossover is produced only in the ultrarelativistic limit $\beta \approx 0.970$). This implies that for practical purposes we can take

$$\begin{aligned}\delta_{\Omega}^{gg}(M_{t\bar{t}}) &= -\operatorname{tr}[\mathbf{C}^{gg}] - 1 \\ &= \frac{75 - 31\beta^2 - (68 - 38\beta^2 + 2\beta^4) \frac{\operatorname{atanh}(\beta)}{\beta}}{-59 + 31\beta^2 + (66 - 36\beta^2 + 2\beta^4) \frac{\operatorname{atanh}(\beta)}{\beta}}\end{aligned}\tag{94}$$

From this expression, we compute the critical top velocity $\beta_c^{\text{PH}} \approx 0.632$ below which the state ρ_{Ω}^{gg} is still entangled, with the associated critical mass being $M_c^{\text{PH}} = 2m_t/\sqrt{1 - \beta_c^2} \approx 446$ GeV.

On the other hand, since $|C_{\perp}^{gg}| > |C_z^{gg}|$, ρ_{Ω}^{gg} can violate the CHSH inequality iff

$$\mu_{\Omega}^{gg} = 2(C_{\perp}^{gg})^2 - 1 > 0\tag{95}$$

This condition is satisfied below the critical value $\beta_c^{\text{CH}} \approx 0.378 < \beta_c^{\text{PH}}$, corresponding to a critical mass $M_c^{\text{CH}} \approx 374$ GeV.

We can also reproduce these results from the spin correlations in the helicity basis. Indeed, since

$$C_{kk}^{gg} + C_{rr}^{gg} = -\frac{50 - (36 - 4\beta^2) \frac{\operatorname{atanh}(\beta)}{\beta}}{-59 + 31\beta^2 + (66 - 36\beta^2 + 2\beta^4) \frac{\operatorname{atanh}(\beta)}{\beta}}\tag{96}$$

we have that $C_{kk}^{gg} + C_{rr}^{gg} < 0$ for $\beta < \beta_{\Delta} \approx 0.864$, and thus, in the energy range where the state is entangled, $\delta_{\Omega}^{gg} = \Delta_{\Omega}^{gg} = -\operatorname{tr}[\mathbf{C}^{gg}] - 1$. In fact, this result can be obtained in any orthonormal basis due to the rotational invariance of the trace, $\operatorname{tr}[\mathbf{C}^{gg}] = 2C_{\perp}^{gg} + C_z^{gg} = C_{rr}^{gg} + C_{nn}^{gg} + C_{kk}^{gg}$, reflecting the symmetry of the spin-singlet state.

However, entanglement is again lost at high energies for ρ_{Ω}^{gg} : even if we use the full Δ_{Ω}^{gg} ,

$$\begin{aligned}\Delta_{\Omega}^{gg} &= \frac{50 - 31\beta^2 - (50 - 36\beta^2 + 2\beta^4) \frac{\operatorname{atanh}(\beta)}{\beta}}{-59 + 31\beta^2 + (66 - 36\beta^2 + 2\beta^4) \frac{\operatorname{atanh}(\beta)}{\beta}} \\ &+ \frac{\left| 25 - (18 - 2\beta^2) \frac{\operatorname{atanh}(\beta)}{\beta} \right|}{-59 + 31\beta^2 + (66 - 36\beta^2 + 2\beta^4) \frac{\operatorname{atanh}(\beta)}{\beta}}\end{aligned}\tag{97}$$

we do not get any entanglement signature, in contrast to $q\bar{q}$ processes. Right Fig. 8 displays all the angular averaged magnitudes for $I = gg$.

3. General considerations

We analyze the global results of Fig. 8 for both processes in the light of the 2D plots of Fig. 3 for $\rho^I(M_{t\bar{t}}, \hat{k})$. The entanglement loss in $\rho_{\Omega}^I(M_{t\bar{t}})$ for both quark and gluon processes arises due to the statistical average over

all possible top directions. However, close to threshold, gluon fusion produces a $t\bar{t}$ pair in a spin singlet [see Eq. (55)], invariant under rotations, and thus unaffected by the angular average, keeping the entanglement.

Nevertheless, an entanglement signature can be recovered for $q\bar{q}$ processes by averaging $\Delta^{q\bar{q}}$, since the helicity basis changes accordingly its orientation to produce a constructive sum of the spin correlations. The same technique does not work for gg production at high energies because there is no entanglement for forward production $\Theta = 0$, which spoils the high p_T entanglement when averaging over all top directions.

D. Mass integration

With the help of the angular averaged PM, it is quite simple to compute integrated values in the region Π of phase space by integrating in the mass range specified by Σ . Since mass integration involves luminosity functions, one has necessarily to consider specific hadron reactions. The angular average of the total PM $R_\Omega(M_{t\bar{t}}, \sqrt{s})$ describing a realistic hadronic $t\bar{t}$ production process for fixed c.m. energy is

$$R_\Omega(M_{t\bar{t}}, \sqrt{s}) = \sum_{I=q\bar{q}, gg} L_I(M_{t\bar{t}}, \sqrt{s}) R_\Omega^I(M_{t\bar{t}}) \quad (98)$$

where we stress that the luminosities $L_I(M_{t\bar{t}}, \sqrt{s})$ only depend on the c.m. energy. The actual spin density matrix $\rho_\Omega(M_{t\bar{t}}, \sqrt{s}) = R_\Omega(M_{t\bar{t}}, \sqrt{s})/4\tilde{A}(M_{t\bar{t}}, \sqrt{s})$ is computed in terms of its partonic counterparts $\rho_\Omega^I(M_{t\bar{t}})$ as in Eq. (59):

$$\rho_\Omega(M_{t\bar{t}}, \sqrt{s}) = \sum_{I=q\bar{q}, gg} w_I(M_{t\bar{t}}, \sqrt{s}) \rho_\Omega^I(M_{t\bar{t}}) \quad (99)$$

where the probabilities $w_I(M_{t\bar{t}}, \sqrt{s})$ are now

$$w_I(M_{t\bar{t}}, \sqrt{s}) = \frac{L_I(M_{t\bar{t}}, \sqrt{s}) \tilde{A}^I(M_{t\bar{t}})}{\sum_J L_J(M_{t\bar{t}}, \sqrt{s}) \tilde{A}^J(M_{t\bar{t}})}. \quad (100)$$

Finally, from Eq. (82), the density matrix ρ_Π reads in terms of these angular averaged magnitudes as

$$\begin{aligned} \rho_\Pi &= \frac{\sum_I \int_\Sigma dM_{t\bar{t}} \frac{\alpha_s^2 \beta}{M_{t\bar{t}}^2} L_I(M_{t\bar{t}}, \sqrt{s}) R_\Omega^I(M_{t\bar{t}})}{\sum_I \int_\Sigma dM_{t\bar{t}} \frac{\alpha_s^2 \beta}{M_{t\bar{t}}^2} L_I(M_{t\bar{t}}, \sqrt{s}) 4\tilde{A}^I(M_{t\bar{t}})} \quad (101) \\ &= \frac{1}{\sigma_\Sigma} \int_\Sigma dM_{t\bar{t}} \frac{d\sigma}{dM_{t\bar{t}}} \rho_\Omega(M_{t\bar{t}}, \sqrt{s}) \end{aligned}$$

with

$$\frac{d\sigma}{dM_{t\bar{t}}} = \int d\Omega \frac{d\sigma}{d\Omega dM_{t\bar{t}}}, \quad \sigma_\Sigma = \int_\Sigma dM_{t\bar{t}} \frac{d\sigma}{dM_{t\bar{t}}} \quad (102)$$

Similar considerations apply to the mass integral of the angular averaged expectation values, such as the spin correlations in the helicity basis.

Because of their illustrative character and their high experimental relevance, we focus on two particular hadronic processes: $p\bar{p}$ collisions at $\sqrt{s} = 2$ TeV (very close to the actual value of $\sqrt{s} = 1.96$ TeV at the Tevatron), and pp collisions at $\sqrt{s} = 13$ TeV (corresponding to the c.m. energy of Run 2 at the LHC). Indeed, as shown in Fig. 5, at the Tevatron $q\bar{q}$ processes dominate while at the LHC gg processes do. The 2D plot of their concurrences is depicted in left column of Fig. 9. We focus on integrating the signal in the two relevant regions for entanglement: close to threshold and at high p_T .

1. Threshold analysis

Close to threshold, the angular results of the previous subsection predict that only gg processes give rise to entangled $t\bar{t}$ pairs. Therefore, we restrict to the LHC example and take $\Sigma = [2m_t, M_{t\bar{t}}]$, which means that only events in the window $[2m_t, M_{t\bar{t}}]$ are selected,

$$\rho(M_{t\bar{t}}, \sqrt{s}) = \frac{1}{\sigma(M_{t\bar{t}})} \int_{2m_t}^{M_{t\bar{t}}} dM \frac{d\sigma}{dM} \rho_\Omega(M, \sqrt{s}) \quad (103)$$

with $\sigma(M_{t\bar{t}})$ the total integrated cross-section in the same mass window. Since it is computed in terms of the angular-averaged sub-states $\rho_\Omega(M_{t\bar{t}}, \sqrt{s})$, the quantum state $\rho(M_{t\bar{t}}, \sqrt{s})$ is also characterized by its integrated transverse and longitudinal spin correlations C_\perp, C_z , represented in Fig. 9b. The necessary and sufficient condition for $\rho_\Omega(M_{t\bar{t}}, \sqrt{s})$ to be entangled is that the integrated value $\delta(M_{t\bar{t}}, \sqrt{s})$ satisfies $\delta(M_{t\bar{t}}, \sqrt{s}) > 0$. Remarkably, this implies that a directly measurable entanglement witness W , which satisfies $W < 0$ only for entangled states [63], is provided by the observable D of Eq. (75),

$$W \equiv D + 1/3 \quad (104)$$

The concurrence is also readily computed from D as $C[\rho] = \max(-1 - 3D, 0)/2$. The integrated value of D (red dashed line) is represented in Fig. 9b, along with the critical value $\beta_c^{\text{PH}}(\sqrt{s})$ (marked by horizontal and vertical solid black lines) below which $W < 0$.

Regarding the CHSH violation, its presence can be signaled by just one parameter, $C_\perp(M_{t\bar{t}}, \sqrt{s})$, through the condition (11), $\mu(M_{t\bar{t}}, \sqrt{s}) = 2[C_\perp(M_{t\bar{t}}, \sqrt{s})]^2 - 1 > 0$. The critical value $\beta_c^{\text{CH}}(\sqrt{s})$ below which there is CHSH violation, $C_\perp(\beta_c^{\text{CH}}, \sqrt{s}) = 1/\sqrt{2}$, is marked in Fig. 9b by horizontal and vertical dashed black lines.

We compute the critical values $\beta_c^{\text{CH}}(\sqrt{s}) \leq \beta_c^{\text{PH}}(\sqrt{s})$ as a function of the c.m. energy, which are represented (dashed red and solid blue, respectively) in Fig. 10. We compare those critical values with those for the angular-averaged sub-states $\rho_\Omega^{gg}(M_{t\bar{t}})$, $\beta_c^{\text{CH}} \approx 0.378 < \beta_c^{\text{PH}} \approx 0.632$ (horizontal dashed and solid lines, respectively). We observe that, for sufficiently large c.m. energies, the critical value $\beta_c^{\text{PH}}(\sqrt{s})$ exceeds its angular-averaged

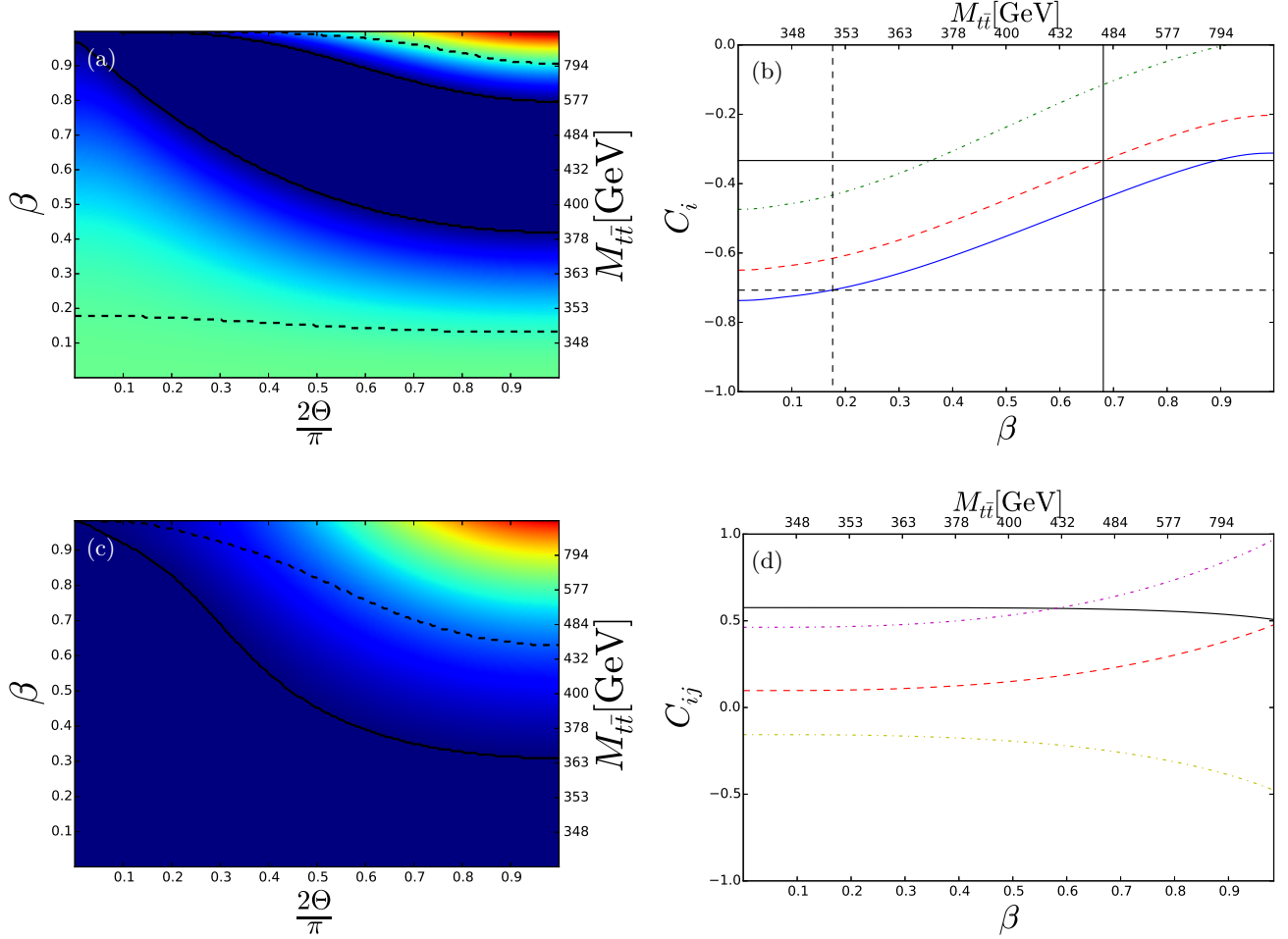


FIG. 9. Upper row: Analysis of $t\bar{t}$ production at the LHC for pp collisions at $\sqrt{s} = 13 \text{ TeV}$. (a) 2D plot of the concurrence as in Figs. 3, 4. (b) Integrated spin correlations C_{\perp} (solid blue) and C_z (dashed dotted green) for $\rho(M_{t\bar{t}})$. The horizontal and vertical solid lines signal the entanglement limit $D = -1/3$ while dashed ones signal the CHSH violation limit $C_{\perp} = 1/\sqrt{2}$. Lower row: Analysis of $t\bar{t}$ production at the Tevatron for $p\bar{p}$ collisions at $\sqrt{s} = 2 \text{ TeV}$. (c) Same as (a). (d) Integrated correlations in the spin helicity basis: C_{rr} (solid black), C_{nn} (dashed yellow), and C_{kk} (dashed-dotted purple). Dashed red line shows the integrated value of Δ .

counterpart, even though $\rho(M_{t\bar{t}}, \sqrt{s})$ contains some mixing with $q\bar{q}$ processes that reduces the entanglement (see lower part of right Fig. 3 and Fig. 9a). This exceeding arises from the fact that the total quantum state $\rho(M_{t\bar{t}}, \sqrt{s})$ is a convex sum of the sub-states $\rho_{\Omega}^I(M_{t\bar{t}})$. Therefore, one needs higher energies to include a sufficient amount of separable states in order to dilute the entanglement. Nevertheless, if the integration window Σ was entirely placed in the region of separability of $\rho_{\Omega}(M_{t\bar{t}})$, no entanglement would be observed. In contrast, for the CHSH violation, $\beta_c^{\text{CH}}(\sqrt{s})$ is below its angular-averaged counterpart, at least within the range of energies considered. This is because of the critical effect introduced by the mixing with $q\bar{q}$ processes at threshold, see Fig. 5. Indeed, for the considered energy of Run 2, $\sqrt{s} = 13 \text{ TeV}$, the weight of gg processes at threshold is barely above the critical value $1/\sqrt{2}$, Fig. 5b.

2. High- p_T analysis

For high p_T at the Tevatron, entanglement is not present in the quantum state ρ_{Π} but is instead signaled by the integrated value of Δ_{Ω} . Indeed, Fig. 9c suggests to choose now the mass window Σ as $[M_{t\bar{t}}, \sqrt{s}]$:

$$\Delta(M_{t\bar{t}}, \sqrt{s}) = \frac{1}{\sigma - \sigma(M_{t\bar{t}})} \int_{M_{t\bar{t}}}^{\sqrt{s}} dM \frac{d\sigma}{dM} \Delta_{\Omega}(M, \sqrt{s}) \quad (105)$$

with σ the total cross-section and $\sigma(M_{t\bar{t}})$ is the integrated cross-section defined after Eq. (103). The value of $\Delta(M_{t\bar{t}}, \sqrt{s})$, along with the integrated helicity spin correlations, is represented in Fig. 9d. Interestingly, even though the $t\bar{t}$ pairs produced close to threshold are not entangled (see lower Fig. 9c), the integration in the mass range makes $\Delta(M_{t\bar{t}}, \sqrt{s}) > 0$ in the whole mass

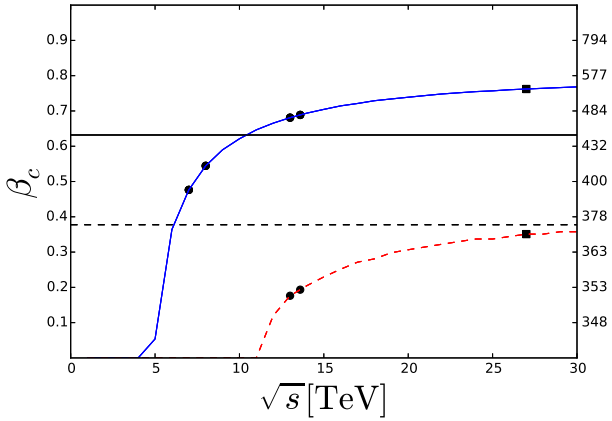


FIG. 10. Critical values $\beta_c^{\text{PH}}(\sqrt{s})$ (solid blue) and $\beta_c^{\text{CH}}(\sqrt{s})$ (dashed red) below which entanglement and CHSH violation can be observed, respectively, close to threshold as a function of the c.m. energy \sqrt{s} for pp collisions. The horizontal lines mark the critical values β_c^{CH} (dashed) and β_c^{PH} (solid) for ρ_{Ω}^{gg} . Black markers indicate the values for c.m. energies of actual high-energy colliders. Circles: Run 1 ($\sqrt{s} = 7, 8$ TeV), Run 2 ($\sqrt{s} = 13$ TeV) and Run 3 ($\sqrt{s} = 13.6$ TeV) of LHC. Squares: Possible upgrade of the LHC ($\sqrt{s} = 27$ TeV).

spectrum, similarly to the increase of the critical values $\beta_c^{\text{CH}}(\sqrt{s}), \beta_c^{\text{PH}}(\sqrt{s})$ for gg processes.

Within the angular averaged scheme considered here, no entanglement can be detected for gg processes at high p_T . We note, however, that entanglement and CHSH violation can be observed at the LHC for high p_T if one also introduces a cut in the top direction, as suggested by Fig. 9a. A detailed analysis of CHSH violation and entanglement in the high p_T region at the same energy of Run 2 is provided in Refs. [41], [42], respectively.

VI. EXPERIMENTAL REMARKS

We complement here the theoretical predictions for observables of the previous section with some experimental remarks about the actual measurement scheme in high-energy colliders, and the potential statistical significance of the discovery. Nevertheless, a dedicated analysis of the expected experimental sensitivity of each prediction is well beyond the scope of the present work.

A. Entanglement detection

The detection of entanglement is more delicate than it could be naively expected from Figs. 3, 4 since, even though entanglement is present in a wide region of phase space, one has to select carefully the phase space regions where the signal is integrated in order to obtain an entanglement signature. In fact, the recent measurement

of the CMS collaboration [38] at the LHC with the data of Run 2, with no restrictions in phase space, yielded no entanglement signature $D = -0.237 \pm 0.011 > -1/3$.

Our analysis reveals that there are two main regions where entanglement can be in principle detected: close to threshold and for high transverse momentum (p_T).

1. Threshold

Close to threshold, as shown in Fig. 5, the only experiment with high enough c.m. energy to give rise to entanglement is the LHC. The idea here is to measure D from the cross-section of Eq. (75), and apply an upper cut in the mass spectrum for the integrated signal. Although our calculation is restricted to LO, in general, the criterion $W = D + 1/3 < 0$ still provides a sufficient condition for the entanglement of $\rho(M_{t\bar{t}})$ without any assumption on its specific form [see Eq. (B8)].

Within this description, the entanglement witness $W < 0$ can be rewritten as the violation of a Cauchy-Schwarz inequality, a typical entanglement signature in other fields such as quantum optics, condensed matter or analog Hawking radiation [45, 64–66]. This is proven by using the P -representation of Eq. (5). If a state is separable, $P(\mathbf{n}_A, \mathbf{n}_B) > 0$, and then

$$\begin{aligned} |\text{tr } \mathbf{C}| &= |\langle \sigma \cdot \sigma \rangle| = \left| \int d\Omega_A d\Omega_B P(\mathbf{n}_A, \mathbf{n}_B) \mathbf{n}_A \cdot \mathbf{n}_B \right| \\ &\leq \int d\Omega_A d\Omega_B P(\mathbf{n}_A, \mathbf{n}_B) |\mathbf{n}_A \cdot \mathbf{n}_B| \\ &\leq \int d\Omega_A d\Omega_B P(\mathbf{n}_A, \mathbf{n}_B) = 1 \end{aligned} \quad (106)$$

Hence, a directly measurable observable as D represents in the range of values $-1 \leq D < -1/3$ a genuine non-classical feature, which can be qualitatively understood from the fact that the classical average of the scalar product of two vectors with unit length is never larger than one, $3|D| = |\text{tr } \mathbf{C}| = |\langle \sigma \cdot \sigma \rangle| \leq 1$. A similar entanglement criterion based on the trace of the correlation matrix was derived for Heisenberg spin chains [67].

A dedicated analysis of the statistical significance of the entanglement discovery was performed in Refs. [40, 42], finding that high-statistical significance can be expected, potentially within 5 statistical deviations (5σ), the standard candle for discovery in high-energy physics.

Finally, Figs. 5, 10 show that the effect of increasing the c.m. energy saturates for large energies. Therefore, we do not expect that future hadron colliders with higher collision energies, such as possible upgrades of the LHC or the FCC, will strongly increase the entanglement in $t\bar{t}$ production. However, we do expect that a larger data collection will enhance the sensitivity of the measurements by reducing the statistical uncertainties. For example, the LHC is expected to collect about 20 times more events with respect to the currently recorded data, while the FCC is expected to collect about 140 times more events.

2. High p_T

For high p_T , both partonic processes $q\bar{q}$ and gg give rise to the same triplet state due to orbital angular momentum dominance. Nevertheless, because the procedure used here averages over all possible top directions, only $q\bar{q}$ processes can yield an entanglement signature. A detailed study of the statistical significance of the possible detection of entanglement for high p_T at the LHC has been already provided in Ref. [42].

In $q\bar{q}$ processes, dominating at the Tevatron, entanglement is detected from the integrated value of Δ , which is in general a sufficient condition for the presence of entanglement [see Eq. (B7)]. There are important conceptual differences between the detection of entanglement close to threshold (involving the measurement of D) and that at high p_T (involving the measurement of Δ). First, close to threshold, entanglement is measured from the direct measurement of one single magnitude, D , while Δ requires the measurement of 3 magnitudes, which are the diagonal spin correlations in the helicity or the diagonal basis. Second, $D + 1/3 < 0$ reveals that the total integrated quantum state ρ_{Π} is entangled, while $\Delta > 0$ signals that some of the substates $\rho(M_{t\bar{t}}, \hat{k}, \sqrt{s})$ are entangled. Thus, we can regard the entanglement detection close to threshold as a stronger quantum signature, measurable from a single magnitude.

At the Tevatron, the relatively low c.m. energy and data recorded yielded high uncertainties on spin-correlation observables [32–34]. Therefore, by considering typical uncertainties of the carried measurements, we do not expect in principle to find an entanglement signature there with high statistical significance.

3. Lorentz invariance

Finally, we would like to discuss the possible role of the reference frame choice on the entanglement detection. While our calculations assume that the $t\bar{t}$ momenta for each production process is well-defined and therefore their entanglement is Lorentz invariant, in realistic situations their wave function is necessarily described by wave packets with finite width, so their entanglement is no longer independent of the reference frame. However, within the current scheme, the $t\bar{t}$ spin polarizations and correlations are by definition measured on their respective rest frames, which are precisely the frames where the lepton directions ℓ_{\pm} are defined through Eq. (69).

B. Quantum tomography

A protocol for the quantum tomography of the $t\bar{t}$ pair was developed in Ref. [40], based on the fact that the experimental procedure of Section V A allows to measure the integrated value of the spin correlations and spin polarizations. Thus, by implementing a cut in the invariant

mass spectrum, one can extract all the relevant parameters characterizing the total quantum state $\rho(M_{t\bar{t}})$ of Eq. (103), which is the basis of quantum tomography. As explained, such a reconstruction requires the use of a fixed orthonormal basis in space, like the beam basis.

We expand here the proposed quantum tomography protocol to more general situations. First, we note that the protocol is not restricted to the state $\rho(M_{t\bar{t}})$, but it is rather valid for any arbitrary integrated quantum state ρ_{Π} by measuring all the 15 parameters B_i^{\pm}, C_{ij} in the beam basis. We can further simplify the process if we integrate over the azimuth around the beam axis, since then rotational invariance is recovered and thus, at LO, only 2 parameters are needed for quantum tomography: the integrated transverse and longitudinal spin correlations C_{\perp}, C_z . In general, by only assuming symmetry around the beam axis, the quantum tomography of the $t\bar{t}$ pair requires the measurement of just 4 parameters, $B_z^{\pm}, C_{\perp}, C_z$, with B_z^{\pm} the spin polarizations along the beam axis. However, from the recent CMS measurement [39], the values of these polarizations are still expected to be quite small. A summary of the parameters needed for the quantum tomography of the $t\bar{t}$ pair is presented in Table I.

Assumption	Coefficients	# parameters
Symmetry and LO	C_{\perp}, C_z	2
Symmetry	$B_z^{\pm}, C_{\perp}, C_z$	4
None	B_i^{\pm}, C_{ij}	15

TABLE I. Summary of the parameters needed to be measured in order to perform the quantum tomography of the $t\bar{t}$ pair for different assumptions on the form of ρ_{Π} . “Symmetry” denotes symmetry around the beam axis, obtained after integration over the azimuth in the beam basis.

Moreover, since the quantum tomography protocol only depends on the decay properties of the $t\bar{t}$ pair and not on the nature of the production process, it can be extended to any $t\bar{t}$ production mechanism, such as e^+e^- collisions. Furthermore, even though we have focused on the case of a dileptonic decay of the $t\bar{t}$ pair, Eqs. (69), (70) are valid for any pair of detectable decay products by just replacing ℓ_{\pm} and $\kappa_{\ell}, \bar{\kappa}_{\ell}$ by the corresponding flight directions in the parent rest frames and spin analyzing powers, respectively. We conclude by noting that the proposed quantum tomography protocol for the $t\bar{t}$ pair goes beyond the general approach to high-energy processes presented in Ref. [56].

C. CHSH violation

Since entanglement is a necessary condition for the violation of CHSH inequalities, CHSH violations are generally expected to be measured with lower statistical significance than entanglement [42]. This is clearly seen by examining the CHSH violation predicted close to thresh-

old at the LHC, Fig. 10, where we see that the upper critical value for a CHSH violation is well below the entanglement one. Remarkably, in a similar fashion to entanglement, the CHSH violation close to threshold is also inferred from the value of just one parameter, C_{\perp} . Nevertheless, one can always measure the full CHSH violation in a more conventional way through Eq. (10). Due to the rotational invariance in the perpendicular plane to the beam, the experimental scheme is similar to the usual case of Bell inequalities with spin singlet states, and one chooses four vectors in that plane $\mathbf{a}_1, \mathbf{a}_2, \mathbf{b}_1, \mathbf{b}_2$ that satisfy $\mathbf{a}_1 \cdot \mathbf{a}_2 = \mathbf{b}_1 \cdot \mathbf{b}_2 = 0$ and $\mathbf{a}_1 \cdot \mathbf{b}_1 = \mathbf{a}_2 \cdot \mathbf{b}_2 = \mathbf{a}_2 \cdot \mathbf{b}_1 = -\mathbf{a}_1 \cdot \mathbf{b}_2 = 1/\sqrt{2}$. Since the correlation matrix should be diagonal in this plane, this experimental scheme is equivalent to measure $C_{\perp} > 1/\sqrt{2}$. We note that our choice of spin directions is fixed *a priori*, so no statistical bias is introduced [42].

Regarding the statistical significance of the CHSH violation close to threshold, we expect it to be much lower than that of entanglement. However, even if a significant detection is not achievable with the current Run 2 data, it could be performed with the increased c.m. energies (as seen from Fig. 10) and larger amount of data provided by future runs and/or colliders. At the Tevatron, since entanglement detection already seems quite challenging, we do not expect to achieve a significant observation of a CHSH violation close to threshold.

As for the case of entanglement, the scheme presented here does not allow to observe CHSH violation at the LHC at high p_T . Nevertheless, a thorough proposal for the detection of CHSH violation in this regime and its statistical significance is presented in Refs. [41, 42].

So far, we have discussed the violation of the CHSH inequality of Eq. (10). Nevertheless, a measurement of a genuine violation of Bell theorem is much more delicate than just measuring some linear combination of spin correlations above certain critical value, like in the case of entanglement. In order to fully rule out a local hidden-variable model, one needs to perform a loophole-free test that ensures that the experimental setup satisfies all the hypotheses of Bell theorem. Loophole-free violations of Bell inequalities were measured for the first time in 2015 [68, 69], and only in 2018 the so-called “free will” loophole was completely closed [70].

Consequently, a careful analysis of the measurement process in a collider is in order. For instance, during Run 2 at the LHC, a bunch of protons collides every 25 ns, yielding typically 60-80 collisions per bunch [71]. The products of these collisions are recorded by different detectors surrounding the pp interaction point that trace the direction and momentum/energy of the collision products. This process goes on for several years during each Run (Run 1 went from 2009 to 2012 and Run 2 went from 2015 to 2018) to collect sufficient amount of statistics.

As a result, in our specific case, the experiments of Alice and Bob should be regarded as the detector recording the $\ell^+\ell^-$ pair resulting from a $t\bar{t}$ pair decay. First, one

needs to ensure that the detection events are causally disconnected. This in principle could be done, since the lepton pair is typically ultrarelativistic due to the large top mass, and moreover causally connected detection events can be rejected after reconstruction of the lepton momenta.

However, a major problem arises due to the fact that the spin directions of the detector cannot be controlled, since we only detect the lepton directions. In fact, technically, one does not even have access to the $t\bar{t}$ spins, but rather infers their expectation values from fitting the cross-section of their decay products. We stress that Eq. (69) is only valid after integrating over all the remaining degrees of freedom of the decay products and cannot be used on an event by event basis. In other words: there is not a measurement setting that yields a ± 1 in each detection event or that can be controlled by Alice or Bob. Therefore, the free-will loophole cannot be closed and even the specific measurement setting of the CHSH inequality is not achievable; only once the spin correlation matrix has been measured from the fit of the differential cross section of the decay products, one can aim at measuring a CHSH violation.

Moreover, many of the events are not useful for the analysis, which gives rise to the so-called detection loophole. The emergence of all these loopholes is quite natural, given that high-energy colliders were not specifically designed for testing Bell inequalities. As a result, in a high-energy collider, we can only detect a *weak* violation of CHSH inequalities, in the sense that some loopholes can never be closed. Related discussions on the validity of Bell tests in high-energy colliders can be found in Refs. [41–43].

VII. CONCLUSIONS AND OUTLOOK

In this work, we have provided the general framework to study the quantum state of a $t\bar{t}$ pair produced in QCD processes. We have discussed that, due to the nature of the measurement process, the quantum state that can be probed in a collider is given in terms of the production spin density matrix. This has to be necessarily a mixed state since a) only momentum measurements are carried out in a collider and b) one has to average over the internal degrees of freedom (like spin or color) of the initial state.

We have analyzed $t\bar{t}$ production for the most elementary QCD partonic reactions. We find that for $q\bar{q}$ processes, entanglement and CHSH violation are equivalent conditions, and are present in whole phase space. For gg processes, entangled $t\bar{t}$ pairs are produced at threshold in a spin singlet state and at high p_T in a spin triplet state. Remarkably, all these features can mostly be understood in terms of basic conservation laws of angular momentum, without invoking the specific details of QCD interactions.

We have shown that, at least at LO, any $t\bar{t}$ production from a real hadronic process can be written in terms of

these basic building blocks through the luminosity functions, which determine the probability of certain partonic reaction at a given c.m. energy in terms of PDF. In particular, we have focused on pp and $p\bar{p}$ collisions, which are those used at the LHC and the Tevatron, respectively. We have performed a detailed analysis on how the $t\bar{t}$ quantum state depends on the c.m. energy of the collisions, finding that at low energies $q\bar{q}$ processes dominate, with the contribution of gg processes increasing with the energy in both cases. For the LHC, gg processes already dominate at the energies of its first run. For the Tevatron, however, due to its relatively low-energy operating point, $q\bar{q}$ processes dominate. Thus, both colliders represent a perfect example of each elementary QCD process.

Thinking in potential experimental realizations, we have proposed a number of realistic observables for the characterization of the $t\bar{t}$ quantum state that provides signatures of entanglement and CHSH violation. Interestingly, these signatures are provided by the measurement of a single magnitude at the LHC: for entanglement, the trace of the correlation matrix is a good entanglement witness, while CHSH violation can be signaled by measuring the spin correlation in the orthogonal plane to the beam.

Finally, we analyze in detail the experimental implementation of these techniques. We show that an entanglement measurement at the LHC represents the violation of a Cauchy-Schwarz inequality. Regarding the Tevatron, we observe that a statistically significant observation of entanglement seems quite challenging due to the relatively large expected uncertainties. We also extend the quantum tomography protocol developed in Ref. [40] to more general quantum states, finding that it can be applied in general to any $t\bar{t}$ quantum state.

Regarding the CHSH violation, since it is a stronger condition than entanglement, its statistical significance is expected to be lower. Moreover, we argue that, due to the nature of the detection process, only weak violations of Bell inequalities can be measured in a high-energy collider, since some loopholes, like those related to the free-will or to the detection efficiency, cannot be closed. This is not surprising, since high-energy colliders were not designed to test Bell inequalities.

From a quantum information perspective, top quarks allow to export fundamental concepts of quantum information, such as entanglement, CHSH violation or quantum tomography, to the high-energy field. This opens the prospect of using high-energy colliders to study quantum information problems at the highest-energy scale available. The genuine relativistic behavior, the exotic character of the interactions and symmetries involved, and the fundamental nature of this environment make it especially attractive for such purpose. Indeed, the detection of entanglement or CHSH violation in $t\bar{t}$ pairs would represent their highest-energy detections ever, many orders of magnitude above standard laboratory setups. Another interesting experiment is the implementation of the quantum tomography of the $t\bar{t}$ pair, which would provide the

highest-energy reconstruction ever of a quantum state, and which could be used for instance to measure quantum discord [72]. A very interesting perspective is provided by the Future Circular Collider, where $t\bar{t}$ pairs are expected to be also produced from collisions of positron-electron (e^+e^-) pairs. Since spin degrees of the initial e^+e^- state can be controlled, in contrast to the QCD production discussed here, the FCC is revealed as a quite promising scenario to study quantum information problems.

From the high-energy perspective, the introduction of quantum information concepts can provide new relevant observables in the field. For example, as inferred from Fig. 4 and ensuing discussion, an entanglement measurement can help to understand the underlying mechanism of a certain production process. A very intriguing extension of this work is to explore New Physics beyond the Standard Model by measuring the quantum state of the $t\bar{t}$ pair, comparing the experimental results with the predictions of the different theories available.

We conclude by stressing that the work has been fully developed within a genuine quantum information framework, since once the production spin density matrix and the luminosity functions are computed by the theory of high-energy physics, all the calculations are reduced to study two-qubit quantum states and incoherent statistical averages between them. Therefore, our work provides a simple and general approach for non-particle physicists to the quantum information aspects of high-energy colliders, a fascinating arena to test the foundations of quantum mechanics.

ACKNOWLEDGMENTS

We thank E. Madge for valuable comments. JR-MdN acknowledges funding from European Union's Horizon 2020 research and innovation programme under the Marie Skłodowska-Curie grant agreement No 847635, and also partially from Grant FIS2017-84368-P from Spain's MINECO.

Appendix A: P -representation and coherent states for qudits

We review here the main properties of the P -representation for qudits introduced in Ref. [73]. We describe a Hilbert space of dimension N as an irreducible representation of $SU(2)$ with angular momentum j such that $N = 2j + 1$. The qudit basis is relabeled as $|jm\rangle$, with $m = -j, -j + 1, \dots, j$ the eigenvalues of the z -component of the angular momentum, $J_z|jm\rangle = m|jm\rangle$. Angular momentum coherent states $|j\hat{\mathbf{n}}\rangle$ are defined as those simultaneously eigenstates of \mathbf{J}^2 and $\mathbf{n} \cdot \mathbf{J}$, i.e., $\mathbf{J}^2 = j(j+1)|j\hat{\mathbf{n}}\rangle$ and $\mathbf{n} \cdot \mathbf{J}|j\hat{\mathbf{n}}\rangle = j|j\hat{\mathbf{n}}\rangle$, where we work in the usual orthonormal basis in spherical coordinates $\{\hat{\mathbf{n}}, \hat{\mathbf{n}}_\theta, \hat{\mathbf{n}}_\phi\}$, with $\hat{\mathbf{n}} = [\sin\theta\cos\phi, \sin\theta\sin\phi, \cos\theta]$, $\hat{\mathbf{n}}_\theta = [\cos\theta\cos\phi, \cos\theta\sin\phi, -\sin\theta]$ and $\hat{\mathbf{n}}_\phi = [-\sin\phi, \cos\phi, 0]$.

We easily compute $|j\hat{\mathbf{n}}\rangle$ from the ladder operators $J_{\pm,\hat{\mathbf{n}}} = \hat{\mathbf{n}}_\theta \cdot \mathbf{J} \pm i\hat{\mathbf{n}}_\phi \cdot \mathbf{J}$ as $J_{+, \hat{\mathbf{n}}} |j\hat{\mathbf{n}}\rangle = 0$, finding

$$|j\hat{\mathbf{n}}\rangle = \sum_{n=0}^{2j} \sqrt{\binom{2j}{n}} \left[\cos \frac{\theta}{2} \right]^{2j-n} \left[\sin \frac{\theta}{2} \right]^n e^{-i(j-n)\phi} |jj-n\rangle \quad (\text{A1})$$

As the more usual coherent states, these states form an overcomplete basis of the Hilbert space,

$$\frac{2j+1}{4\pi} \int d\Omega |j\hat{\mathbf{n}}\rangle \langle j\hat{\mathbf{n}}| = \sum_m |jm\rangle \langle jm| = I_{2j+1} \quad (\text{A2})$$

The P -representation is defined from these coherent states as

$$\rho = \int d\Omega P(\hat{\mathbf{n}}) |j\hat{\mathbf{n}}\rangle \langle j\hat{\mathbf{n}}|, \quad \int d\Omega P(\hat{\mathbf{n}}) = 1 \quad (\text{A3})$$

This definition does not completely fix $P(\hat{\mathbf{n}})$. In order to check it, we consider its expansion in spherical harmonics

$$P(\hat{\mathbf{n}}) = \sum_{\ell=0}^{\infty} \sum_{m=-\ell}^{\ell} p_{\ell m} Y_\ell^m(\hat{\mathbf{n}}) \quad (\text{A4})$$

$$Y_\ell^m(\hat{\mathbf{n}}) = \sqrt{\frac{2\ell+1}{4\pi} \frac{(\ell-m)!}{(\ell+m)!}} \sin^m \theta P_\ell^m(\cos \theta) e^{im\phi}$$

where $P_\ell^m(\cos \theta)$ are the associated Legendre polynomials. Normalization of $P(\hat{\mathbf{n}})$ implies $p_{00} = 1/\sqrt{4\pi}$. Since spherical harmonics form an orthonormal basis, when inserting Eq. (A1) in Eq. (A3) we realize that only the coefficients $p_{\ell m}$ with $\ell \leq 2j$ are involved, while those for $\ell > 2j$ remain undetermined. Thus, the most general expression for $P(\hat{\mathbf{n}})$ is

$$P(\hat{\mathbf{n}}) = \frac{1}{4\pi} + \sum_{\ell=1}^{2j} \sum_{m=-\ell}^{\ell} p_{\ell m} Y_\ell^m(\hat{\mathbf{n}}) + Q_{2j} f(\hat{\mathbf{n}}) \quad (\text{A5})$$

with Q_{2j} the projector onto $\ell > 2j$ and $f(\hat{\mathbf{n}})$ an arbitrary angular function. Since $P(\hat{\mathbf{n}})$ is a real function, the number of real parameters determining the coefficients $\{p_{\ell m}\}_{\ell=1}^{2j}$ is precisely $(2j+1)^2 - 1 = 4j(j+1)$, the number of parameters fixing an arbitrary density matrix ρ in a Hilbert space of dimension $2j+1$. Therefore, any density matrix can be described in terms of a certain function $P(\hat{\mathbf{n}})$, where classical states are those admitting a non-negative P function.

We now focus on the main case of the paper, where $j = 1/2$. For a qubit, the coherent states are the usual spin states

$$|\hat{\mathbf{n}}\rangle = \cos \frac{\theta}{2} e^{-i\frac{\phi}{2}} |\uparrow\rangle + \sin \frac{\theta}{2} e^{i\frac{\phi}{2}} |\downarrow\rangle \quad (\text{A6})$$

where $|\uparrow\rangle, |\downarrow\rangle$ are the spin states along the z -axis $|\frac{1}{2} \pm \frac{1}{2}\rangle$. Since $2j = 1$, only spherical harmonics up to $\ell = 1$ in the expansion of $P(\hat{\mathbf{n}})$ are involved in the expression of ρ . This can be straightforwardly seen by noticing in Eq. (2) that

$$|\mathbf{n}\rangle \langle \mathbf{n}| = \frac{1 + \mathbf{n} \cdot \boldsymbol{\sigma}}{2} \quad (\text{A7})$$

Moreover, if we choose the $i = x, y, z$ basis for the spherical harmonics $Y_i^1(\hat{\mathbf{n}}) = \sqrt{\frac{3}{4\pi}} \hat{n}_i$, we simply find that the B_i coefficients of Eq. (1) are

$$B_i = \sqrt{\frac{4\pi}{3}} p_{1i} \quad (\text{A8})$$

and thus

$$P(\hat{\mathbf{n}}) = \frac{1}{4\pi} [1 + 3\mathbf{B} \cdot \hat{\mathbf{n}}] + Q_1 f(\hat{\mathbf{n}}) \quad (\text{A9})$$

For one qubit, a non-negative $P(\hat{\mathbf{n}})$ can always be found since ρ is in fact an incoherent mixture of the two spin states along the direction of \mathbf{B} .

For a two-qubit system, things are straightforwardly adapted from the one qubit case. In particular, the most general expression for $P(\hat{\mathbf{n}}_A, \hat{\mathbf{n}}_B)$, defined through Eq. (5), is now

$$P(\hat{\mathbf{n}}_A, \hat{\mathbf{n}}_B) = \frac{1}{(4\pi)^2} [1 + 3\mathbf{B}^+ \cdot \hat{\mathbf{n}}_A + 3\mathbf{B}^- \cdot \hat{\mathbf{n}}_B \quad (\text{A10}) \\ + 9 \hat{\mathbf{n}}_A \cdot \mathbf{C} \cdot \hat{\mathbf{n}}_B] + Q_1 \otimes Q_1 f(\hat{\mathbf{n}}_A, \hat{\mathbf{n}}_B)$$

Entangled states are thus states for which no $f(\hat{\mathbf{n}}_A, \hat{\mathbf{n}}_B)$ can be found such that $P(\hat{\mathbf{n}}_A, \hat{\mathbf{n}}_B)$ is non-negative.

Appendix B: Specific entanglement criteria for $t\bar{t}$ pairs

We derive here some adapted results for $t\bar{t}$ quantum states from the general entanglement criteria discussed in Section II A. For that purpose, we write the full matrix form of the general expression of a density matrix ρ in a 2×2 Hilbert space, Eq. (4):

$$\rho = \frac{1}{4} \begin{bmatrix} 1 + B_3^+ + B_3^- + C_{33} & B_1^- + C_{31} - i(B_2^- + C_{32}) & B_1^+ + C_{13} - i(B_2^+ + C_{23}) & C_{11} - C_{22} - i(C_{12} + C_{21}) \\ B_1^- + C_{31} + i(B_2^- + C_{32}) & 1 + B_3^+ - B_3^- - C_{33} & C_{11} + C_{22} + i(C_{12} - C_{21}) & B_1^+ - C_{13} - i(B_2^+ - C_{23}) \\ B_1^+ + C_{13} + i(B_2^+ + C_{23}) & C_{11} + C_{22} + i(C_{21} - C_{12}) & 1 - B_3^+ + B_3^- - C_{33} & B_1^- - C_{31} - i(B_2^- - C_{32}) \\ C_{11} - C_{22} + i(C_{21} + C_{12}) & B_1^+ - C_{13} + i(B_2^+ - C_{23}) & B_1^- - C_{31} + i(B_2^- - C_{32}) & 1 - B_3^+ - B_3^- + C_{33} \end{bmatrix} \quad (\text{B1})$$

where we are following the usual convention for the expression of the Pauli matrices σ_i . For the analysis of the Peres-Horodecki criterion, we compute the partial transpose of ρ with respect to the second subsystem, ρ^{T_2} , which amounts to transpose the $4 \times 2 \times 2$ blocks, namely:

$$\rho^{\text{T}_2} = \frac{1}{4} \begin{bmatrix} 1 + B_3^+ + B_3^- + C_{33} & B_1^- + C_{31} + i(B_2^- + C_{32}) & B_1^+ + C_{13} - i(B_2^+ + C_{23}) & C_{11} + C_{22} + i(C_{12} - C_{21}) \\ B_1^- + C_{31} - i(B_2^- + C_{32}) & 1 + B_3^+ - B_3^- - C_{33} & C_{11} - C_{22} - i(C_{12} + C_{21}) & B_1^+ - C_{13} - i(B_2^+ - C_{23}) \\ B_1^+ + C_{13} + i(B_2^+ + C_{23}) & C_{11} - C_{22} + i(C_{21} + C_{12}) & 1 - B_3^+ + B_3^- - C_{33} & B_1^- - C_{31} + i(B_2^- - C_{32}) \\ C_{11} + C_{22} + i(C_{21} - C_{12}) & B_1^+ - C_{13} + i(B_2^+ - C_{23}) & B_1^- - C_{31} - i(B_2^- - C_{32}) & 1 - B_3^+ - B_3^- + C_{33} \end{bmatrix} \quad (\text{B2})$$

The Peres-Horodecki criterion states that ρ^{T_2} is non-negative iff ρ is separable. A simpler version of this statement is obtained by considering vectors with only first and fourth component, which gives a reduced quadratic form

$$\rho_C \equiv \begin{bmatrix} 1 + B_3^+ + B_3^- + C_{33} & C_{11} + C_{22} + i(C_{12} - C_{21}) \\ C_{11} + C_{22} + i(C_{21} - C_{12}) & 1 - B_3^+ - B_3^- + C_{33} \end{bmatrix} \quad (\text{B3})$$

The non-negative character of ρ^{T_2} implies $\det \rho_C \geq 0$. Thus, $\det \rho_C < 0$ is a *sufficient* condition of entanglement since it implies that ρ^{T_2} is not non-negative. It can be rewritten as $\mathcal{P} > 0$, with

$$\mathcal{P} \equiv (B_3^+ + B_3^-)^2 + (C_{11} + C_{22})^2 + (C_{21} - C_{12})^2 - (1 + C_{33})^2 \quad (\text{B4})$$

Furthermore,

$$\mathcal{P} \geq (C_{11} + C_{22})^2 - (1 + C_{33})^2 \equiv \tilde{\mathcal{P}}, \quad (\text{B5})$$

so $\tilde{\mathcal{P}} > 0$ provides an even simpler entanglement criterion. Specifically, since $1 + C_{33} \geq 0$, $\tilde{\mathcal{P}} > 0$ iff

$$|C_{11} + C_{22}| > 1 + C_{33} \quad (\text{B6})$$

Thus, the entanglement signatures used in the main text

$$\Delta \equiv \frac{-C_{33} + |C_{11} + C_{22}| - 1}{2} > 0 \quad (\text{B7})$$

as well as

$$W = D + \frac{1}{3} \equiv \frac{\text{tr}[\mathbf{C}]}{3} + \frac{1}{3} < 0 \quad (\text{B8})$$

are sufficient conditions for entanglement in general, valid for arbitrary quantum state in 2×2 bipartite Hilbert spaces.

We now address the specific case of the main text of $t\bar{t}$ production through LO QCD, for which we assume unpolarized quantum states, $B_i^+ = B_i^- = 0$, and a symmetric correlation matrix is symmetric, $C_{ij} = C_{ji}$. The latter condition implies that the correlation matrix can be diagonalized after the appropriated rotation, $C = \text{diag}[C_1, C_2, C_3]$, which reduces Eq. (B1) to

$$\rho = \frac{1}{4} \begin{bmatrix} 1 + C_3 & 0 & 0 & C_1 - C_2 \\ 0 & 1 - C_3 & C_1 + C_2 & 0 \\ 0 & C_1 + C_2 & 1 - C_3 & 0 \\ C_1 - C_2 & 0 & 0 & 1 + C_3 \end{bmatrix} \quad (\text{B9})$$

It is easy to see that

$$\pm C_3 + |C_1 \pm C_2| - 1 \leq 0 \quad (\text{B10})$$

by demanding ρ to be a physical state described by a non-negative operator. This complements the Peres-Horodecki criterion, which says that the state is entangled iff

$$\pm C_3 + |C_1 \mp C_2| - 1 > 0 \quad (\text{B11})$$

By combining both conditions, we find that Peres-Horodecki is equivalent to

$$\begin{aligned} -C_3 + |C_1 + C_2| - 1 &> 0, & C_3 \leq 0 \\ C_3 + |C_1 - C_2| - 1 &> 0, & C_3 \geq 0 \end{aligned} \quad (\text{B12})$$

where the first line is just the condition $\Delta > 0$ of Eq. (B7).

In the particular case of Eq. (B9) where ρ is real and unpolarized, the concurrence can be also analytically computed from its definition (8), since in that case $\tilde{\rho} = \rho$. Hence, $\sqrt{\sqrt{\rho}\tilde{\rho}\sqrt{\rho}} = \rho$, and λ_i are the eigenvalues of ρ , $\lambda_i = \frac{1}{4}(1 + C_3 \pm |C_1 - C_2|)$, $\frac{1}{4}(1 - C_3 \pm |C_1 + C_2|)$. Moreover, since ρ has unit trace,

$$\sum_i \lambda_i = 1, \quad (\text{B13})$$

and the concurrence is simply $C[\rho] = \max(2\lambda_1 - 1, 0)$, with $2\lambda_1 - 1 = (\pm C_3 + |C_1 \mp C_2| - 1)/2$. By noting the analogy with Eq. (B11), we can write the concurrence directly in terms of the Peres-Horodecki criterion:

$$\begin{aligned} C[\rho] &= \frac{1}{2} \max[-C_3 + |C_1 + C_2| - 1, 0], & C_3 \leq 0 \\ C[\rho] &= \frac{1}{2} \max[C_3 + |C_1 - C_2| - 1, 0], & C_3 \geq 0 \end{aligned} \quad (\text{B14})$$

For the study of the integrated quantum states along all top directions, ρ_Ω , we consider the particular case in which there is invariance under rotations around a certain direction, chosen along σ_3 and labeled as the z -axis.

In that case, the spin polarizations must be longitudinal, $B_i^\pm = B_z^\pm \delta_{i3}$, and the correlation matrix is diagonal, $C_{ij} = \delta_{ij} C_j$, with eigenvalues $C_1 = C_2 = C_\perp$ and $C_3 = C_z$. The Peres-Horodecki criterion is then equivalent to

$$4C_\perp^2 + (B_z^+ + B_z^-)^2 - (1 + C_z)^2 > 0 \quad (\text{B15})$$

If the state is unpolarized,

$$\delta \equiv \frac{-C_z + 2|C_\perp| - 1}{2} > 0 \quad (\text{B16})$$

is a necessary and sufficient condition for entanglement, while for $B_z^\pm \neq 0$, $\delta > 0$ is just a sufficient condition.

Appendix C: Parton distribution functions

We further explain here the concept of PDF and detail how the luminosity functions $L^I(M_{t\bar{t}}, \sqrt{s})$ of Eq. (57) are computed. The PDF $N_\pi(x)$ determines the probability of originating a parton π from one of the hadrons with an energy fraction $0 \leq x \leq 1$. For instance, in the case of pp collisions, a $t\bar{t}$ pair is originated from the collision of a parton π from one of the protons and the corresponding antiparton $\bar{\pi}$ from the other proton. The probability of producing a state $I = \pi\bar{\pi}$ with partonic c.m. energy $\hat{s} = x_1 x_2 \sqrt{s}$ is $N_\pi(x_1)N_{\bar{\pi}}(x_2)$. In the case of $I = gg$, π is a gluon. In the case of $I = q\bar{q}$, π can be some light quark, $\pi = u, d, c, s, b$, or their respective antiparticles $\bar{u}, \bar{d}, \bar{c}, \bar{s}, \bar{b}$. Since the partonic c.m. frame is that of the $t\bar{t}$ pair, the c.m. energy is the same, $M_{t\bar{t}} = \sqrt{\hat{s}}$, and thus we can compute the luminosity function as

$$L_I(M_{t\bar{t}}, s) = \sum_{\pi} \int_0^1 \int_0^1 dx_1 dx_2 \delta(M_{t\bar{t}} - \sqrt{\hat{s}}) N_\pi(x_1) N_{\bar{\pi}}(x_2) \quad (\text{C1})$$

where the index π labels all the possible partons giving rise to the state I . Changing to the dimensionless variables $x = \sqrt{x_1 x_2} = M_{t\bar{t}}/\sqrt{s}$, $t = \sqrt{x_1/x_2}$ gives

$$L_I(M_{t\bar{t}}, s) = \sum_{\pi} \frac{2x}{\sqrt{s}} \int_x^{\frac{1}{x}} \frac{dt}{t} N_\pi(xt) N_{\bar{\pi}}\left(\frac{x}{t}\right) \quad (\text{C2})$$

For the case of $p\bar{p}$ collisions, we simply replace one of the proton PDF above by the antiproton PDF $\bar{N}_\pi(x)$, which is that of the proton but interchanging partons with antipartons, $\bar{N}_\pi(x) = N_{\bar{\pi}}(x)$.

The luminosity integral (C2) is computed numerically, using the PDF values proportioned by the NNPDF30LO

PDF set [74]. No significant change is found if other PDF sets are used.

Appendix D: Angular averaging

We outline here the main technical details about the computation of the angular integrals presented in Section V C.

a. $q\bar{q}$ production

For computing the angular averages involved in $q\bar{q}$ production, the polar integrals in Θ can be computed either as polynomials in $t = \cos \Theta$ or in terms of

$$F_n \equiv \int_0^{\frac{\pi}{2}} d\Theta \sin^n \Theta = \frac{n-1}{n} I_{n-2} = \frac{\Gamma\left(\frac{n+1}{2}\right)}{\Gamma\left(\frac{n+2}{2}\right)} \frac{\sqrt{\pi}}{2} \quad (\text{D1})$$

with $\Gamma(x)$ the usual Euler gamma function.

b. gg production

Computations of angular averages in gg processes are more elaborated. Nevertheless, it can be seen that all the involved integrals can be put in terms of $K_{n,2}(\beta)$, with

$$K_{n,m}(x) \equiv \int_{-x}^x dz \frac{z^{2n}}{(1-z^2)^m} \quad (\text{D2})$$

This integral satisfies recursion relations

$$K_{n,m}(x) = K_{n-1,m}(x) - K_{n-1,m-1}(x) \quad (\text{D3})$$

$$\begin{aligned} K_{n,0}(x) &= 2 \frac{x^{2n+1}}{2n+1} \\ K_{0,m}(x) &= \frac{1}{(m-1)} \left[\frac{x}{(1-x^2)^{m-1}} + \frac{2m-3}{2} K_{0,m-1}(x) \right] \\ K_{0,1}(x) &= 2 \operatorname{atanh}(x) = \ln \frac{1+x}{1-x} \end{aligned}$$

that eventually yield

$$\begin{aligned} K_{n,1}(x) &= 2 \left[\operatorname{atanh}(x) - \sum_{k=0}^{n-1} \frac{x^{2k+1}}{2k+1} \right] \\ K_{n,2}(x) &= \frac{x}{1-x^2} - (2n-1) \operatorname{atanh}(x) \\ &+ \sum_{k=0}^{n-2} \frac{2(n-1-k)}{2k+1} x^{2k+1} \end{aligned} \quad (\text{D4})$$

[1] A. Einstein, B. Podolsky, and N. Rosen, Phys. Rev. **47**, 777 (1935).
[2] E. Schrodinger, Pro. Cambridge Phi. Soc. **31**, 555 (1935).
[3] J. S. Bell, Physics Physique Fizika **1**, 195 (1964).
[4] C. H. Bennett, G. Brassard, C. Crépeau, R. Jozsa, A. Peres, and W. K. Wootters, Phys. Rev. Lett. **70**, 1895 (1993).
[5] D. Bouwmeester, J.-W. Pan, K. Mattle, M. Eibl, H. Weinfurter, and A. Zeilinger, Nature **390**, 575 (1997).

[6] D. Gottesman and I. L. Chuang, *Nature* **402**, 390 (1999).

[7] C. H. Bennett and D. P. DiVincenzo, *Nature* **404**, 247 (2000).

[8] R. Raussendorf and H. J. Briegel, *Phys. Rev. Lett.* **86**, 5188 (2001).

[9] N. Gisin, G. Ribordy, W. Tittel, and H. Zbinden, *Rev. Mod. Phys.* **74**, 145 (2002).

[10] V. Giovannetti, S. Lloyd, and L. Maccone, *Science* **306**, 1330 (2004).

[11] R. M. Gingrich and C. Adami, *Phys. Rev. Lett.* **89**, 270402 (2002).

[12] A. Peres and D. R. Terno, *Rev. Mod. Phys.* **76**, 93 (2004).

[13] N. Friis, R. A. Bertlmann, M. Huber, and B. C. Hiesmayr, *Phys. Rev. A* **81**, 042114 (2010).

[14] N. Friis, A. R. Lee, K. Truong, C. Sabín, E. Solano, G. Johansson, and I. Fuentes, *Phys. Rev. Lett.* **110**, 113602 (2013).

[15] F. Giacomini, E. Castro-Ruiz, and i. c. v. Brukner, *Phys. Rev. Lett.* **123**, 090404 (2019).

[16] A. Bramon and G. Garbarino, *Phys. Rev. Lett.* **88**, 040403 (2002).

[17] Y. Shi, *Phys. Rev. D* **70**, 105001 (2004).

[18] B. Kayser, J. Kopp, R. G. H. Robertson, and P. Vogel, *Phys. Rev. D* **82**, 093003 (2010).

[19] A. Cervera-Lierta, J. I. Latorre, J. Rojo, and L. Rottoli, *SciPost Phys.* **3**, 036 (2017).

[20] Z. Tu, D. E. Kharzeev, and T. Ullrich, *Phys. Rev. Lett.* **124**, 062001 (2020).

[21] X. Feal, C. Pajares, and R. A. Vazquez, *Phys. Rev. C* **104**, 044904 (2021).

[22] S. Abachi *et al.* (D0), *Phys. Rev. Lett.* **74**, 2632 (1995), arXiv:hep-ex/9503003.

[23] F. Abe *et al.* (CDF), *Phys. Rev. Lett.* **74**, 2626 (1995), arXiv:hep-ex/9503002.

[24] G. L. Kane, G. A. Ladinsky, and C. P. Yuan, *Phys. Rev. D* **45**, 124 (1992).

[25] W. Bernreuther and A. Brandenburg, *Phys. Rev. D* **49**, 4481 (1994).

[26] S. Parke and Y. Shadmi, *Physics Letters B* **387**, 199 (1996).

[27] W. Bernreuther, M. Flesch, and P. Haberl, *Phys. Rev. D* **58**, 114031 (1998).

[28] W. Bernreuther, A. Brandenburg, Z. Si, and P. Uwer, *Nuclear Physics B* **690**, 81 (2004).

[29] P. Uwer, *Physics Letters B* **609**, 271 (2005).

[30] M. Baumgart and B. Tweedie, *Journal of High Energy Physics* **2013**, 117 (2013).

[31] W. Bernreuther, D. Heisler, and Z.-G. Si, *Journal of High Energy Physics* **2015**, 1 (2015).

[32] T. Aaltonen *et al.* (CDF), *Phys. Rev. D* **83**, 031104 (2011), arXiv:1012.3093 [hep-ex].

[33] V. M. Abazov *et al.* (D0), *Phys. Rev. Lett.* **107**, 032001 (2011), arXiv:1104.5194 [hep-ex].

[34] V. M. Abazov *et al.* (D0), *Phys. Lett. B* **757**, 199 (2016), arXiv:1512.08818 [hep-ex].

[35] G. Aad *et al.* (ATLAS), *Phys. Rev. Lett.* **108**, 212001 (2012), arXiv:1203.4081 [hep-ex].

[36] S. Chatrchyan *et al.* (CMS), *Phys. Rev. Lett.* **112**, 182001 (2014), arXiv:1311.3924 [hep-ex].

[37] G. Aad *et al.* (ATLAS), *Phys. Rev. Lett.* **114**, 142001 (2015), arXiv:1412.4742 [hep-ex].

[38] A. M. Sirunyan *et al.* (CMS), *Phys. Rev. D* **100**, 072002 (2019), arXiv:1907.03729 [hep-ex].

[39] M. Aaboud *et al.* (ATLAS), *Eur. Phys. J. C* **80**, 754 (2020), arXiv:1903.07570 [hep-ex].

[40] Y. Afik and J. R. M. n. de Nova, *Eur. Phys. J. Plus* **136**, 907 (2021), arXiv:2003.02280 [quant-ph].

[41] M. Fabbrichesi, R. Floreanini, and G. Panizzo, *Phys. Rev. Lett.* **127**, 161801 (2021).

[42] C. Severi, C. D. E. Boschi, F. Maltoni, and M. Sioli, “Quantum tops at the lhc: from entanglement to bell inequalities,” (2021), arXiv:2110.10112 [hep-ph].

[43] A. J. Barr, *Physics Letters B* **825**, 136866 (2022).

[44] A. J. Larkoski, “A general analysis for observing quantum interference at colliders,” (2022), arXiv:2201.03159 [hep-ph].

[45] D. Walls and G. Milburn, *Quantum Optics*, Springer-Link: Springer e-Books (Springer, 2008).

[46] A. Peres, *Phys. Rev. Lett.* **77**, 1413 (1996).

[47] P. Horodecki, *Physics Letters A* **232**, 333 (1997).

[48] W. K. Wootters, *Phys. Rev. Lett.* **80**, 2245 (1998).

[49] D. F. V. James, P. G. Kwiat, W. J. Munro, and A. G. White, *Phys. Rev. A* **64**, 052312 (2001).

[50] J. F. Clauser, M. A. Horne, A. Shimony, and R. A. Holt, *Phys. Rev. Lett.* **23**, 880 (1969).

[51] R. Horodecki, P. Horodecki, and M. Horodecki, *Physics Letters A* **200**, 340 (1995).

[52] B. S. Cirel'son, *Letters in Mathematical Physics* **4**, 93 (1980).

[53] J. Taylor, *Scattering Theory: The Quantum Theory of Nonrelativistic Collisions*, Dover Books on Engineering (Dover Publications, 2012).

[54] We note that this definition differs from that of Ref. [40] by a factor 2, since in this way $\Delta^I \leq 1$.

[55] D. E. Kharzeev and E. M. Levin, *Phys. Rev. D* **95**, 114008 (2017).

[56] J. C. Martens, J. P. Ralston, and J. T. Takaki, *The European Physical Journal C* **78**, 5 (2018).

[57] We note that the result for $\Delta^{q\bar{q}}$ in Ref. [40] contained a typo, and a factor 2 was missing.

[58] G. Mahlon and S. Parke, *Phys. Rev. D* **53**, 4886 (1996).

[59] R. Feynman, *Conf. Proc. C* **690905**, 237 (1969).

[60] J. Bjorken and E. A. Paschos, *Phys. Rev.* **185**, 1975 (1969).

[61] P. Azzi *et al.*, *CERN Yellow Rep. Monogr.* **7**, 1 (2019), arXiv:1902.04070 [hep-ph].

[62] M. Benedikt, A. Blondel, P. Janot, M. Mangano, and F. Zimmermann, *Nature Phys.* **16**, 402 (2020).

[63] B. M. Terhal, *Physics Letters A* **271**, 319 (2000).

[64] S. Wölk, M. Huber, and O. Gühne, *Phys. Rev. A* **90**, 022315 (2014).

[65] J. R. M. de Nova, F. Sols, and I. Zapata, *Phys. Rev. A* **89**, 043808 (2014).

[66] J. R. M. de Nova, F. Sols, and I. Zapata, *New Journal of Physics* **17**, 105003 (2015).

[67] J. Schliemann, *Phys. Rev. A* **68**, 012309 (2003).

[68] B. Hensen, H. Bernien, A. E. Dréau, A. Reiserer, N. Kalb, M. S. Blok, J. Ruitenberg, R. F. Vermeulen, R. N. Schouten, C. Abellán, *et al.*, *Nature* **526**, 682 (2015).

[69] M. Giustina, M. A. M. Versteegh, S. Wengerowsky, J. Handsteiner, A. Hochrainer, K. Phelan, F. Steinlechner, M. Neuenschwander, N. K. Langford, A. K. Albrecht, C. Kurtsiefer, and A. Zeilinger, *Nature* **526**, 682 (2015).

ner, J. Kofler, J.-A. Larsson, C. Abellán, W. Amaya, V. Pruneri, M. W. Mitchell, J. Beyer, T. Gerrits, A. E. Lita, L. K. Shalm, S. W. Nam, T. Scheidl, R. Ursin, B. Wittmann, and A. Zeilinger, Phys. Rev. Lett. **115**, 250401 (2015).

[70] BIG Bell Test Collaboration, Nature (London) **557**, 212 (2018), arXiv:1805.04431 [quant-ph].

[71] G. Aad *et al.* (ATLAS), JINST **15**, P10004 (2020), arXiv:2007.12539 [physics.ins-det].

[72] H. Ollivier and W. H. Zurek, Phys. Rev. Lett. **88**, 017901 (2001).

[73] O. Giraud, P. Braun, and D. Braun, Phys. Rev. A **78**, 042112 (2008).

[74] R. D. Ball *et al.* (NNPDF), JHEP **04**, 040 (2015), arXiv:1410.8849 [hep-ph].